of benzoquinones (the main reactive metabolites of trichlorobenzenes) was effectively detected with the *S. typhimurium* strains TA104 and TA2637. TA104 was most sensitive to oxidative mutagens, while TA2637 was effective in detecting bulky DNA adducts.

(2) Different activity levels of the specific enzymes in rats and mice responsible for the metabolic activation of chlorinated benzenes. According to the investigation of Hissink et al., the rank order for total in vitro conversion of chlorobenzenes to oxidized metabolites and covalently bound metabolites was mouse > rat ≫ human.[72] Moreover, conversion-dependent covalent binding to proteins was observed for all chlorinated benzenes, in which benzoquinones amounted to about 10−30% of the total metabolites formed.[73] Den Besten et al.[74] were found that cytochrome P4503A1 showed the highest activity toward trichlorobenzenes both with regard to the formation of corresponding chlorophenols and protein-bound metabolites. Thus, the activity of CYP3A1 strain to produce reactive benzoquinone metabolites from trichlorobenzenes seems to be higher in mice than in rats.

The critical review of the observed genotoxicity within the list of 162 workflow chemicals has changed the MNT predicted outcome of some of the "original" 557 training set chemicals. Thus, after including the in vivo metabolic detoxification "logic", the newly developed MNT model exhibited an improved performance: sensitivity of 82% (i.e., 217 correctly predicted genotoxic chemicals out of the total number of 266 documented genotoxins), specificity of 61% (i.e., 170 correctly predicted nongenotoxic chemicals out of total number of 281 observed nongenotoxins), and concordance of 71%. To calculate the model concordance, the chemicals for which explicit model prediction could not be provided (there were 10 chemicals that failed to achieve the user defined threshold of 70%) were excluded from the "557 list". Thus, the model concordance of 71% is based on relation between the total number of correct predictions (genotoxic and nongenotoxic, i.e., 387) out of 547 chemicals.

Derivation of the Model for in Vivo Liver Genotoxicity. The modeling of in vivo liver genotoxicity is based on documented data effects for 185 diverse chemicals assessed by the UDS, Comet, and TGR assays (Appendix III in the Supporting Information). The model shared the reactivity and, to a certain extent, the metabolism components of the in vivo MNT model. On the basis of the selection of liver as the target organ of this investigation, the "bioexhausting" component of the detoxification stage usually associated with targets (such as bone marrow) remote from the liver is not considered herein. The liver model was derived directly following the logic of the workflow presented in Figure 1. According to this logic, two possible genotoxicity outcomes are feasible for the in vitro nonmutagenic chemicals. Most of these in vitro negative chemicals are not expected to elicit in vivo liver genotoxicity, whereas bioactivation reactions producing liver damaging metabolites can occur for a limited set of nonmutagens. The fate of the in vitro mutagenic chemicals was also implemented in this logic. Thus, for some in vitro mutagens (e.g., aromatic amines possessing polar functional groups), the parent chemicals or their metabolites or both could be "trapped" in liver detoxification pathways; as a result, they will not elicit genotoxic effect in the target organ. For example, *p*-aminobenzoic acid is found to be liver nongenotoxic, being readily absorbed by the gastrointestinal tract.[75] The liver is the principle site of glycine phase II conjugation; thus, this chemical was not subjected to N-hydroxylation phase I bioactivation reactions such as aromatic amine N-hydroxylation. Bearing in mind metabolic consideration mainly, if in vitro mutagenic chemicals were not involved in liver "trapping" detoxification, they would be considered to be in vivo liver genotoxins. At the present time, 76 "trapping" detoxification pathways have been implemented into the liver genotoxicity model and contribute to its sensitivity of 85% (i.e., 90 correctly predicted genotoxic chemicals of 106 observed liver genotoxins) and specificity of 49% (i.e., 35 correctly predicted nongenotoxic chemicals of 72 observed nongenotoxins). Seven chemicals for which the model cannot provide explicit predictions were excluded from the model statistics. The poor specificity is attributed to the fact that the model was derived in the progression of our in vitro−in vivo investigation, and thus, identification of new "trapping" detoxification pathways according to the "185" list of chemicals is needed before this model is really acceptable for use. This search is ongoing. Some of the most commonly applied "trapping" pathways in detoxification on training set chemicals are as follows:

- Nitroarene reduction → N-acetylation pathway,
- Oxidative O-dealkylation → glucuronidation pathway,
- Oxidative O-dealkylation → sulfation pathway,
- Epoxide hydration → glutathione conjugation pathway, etc.

The nitroarene reduction → N-acetylation pathway is involved in the liver "trapping" detoxification of 4-nitrobenzoic acid as illustrated in Figure 12.

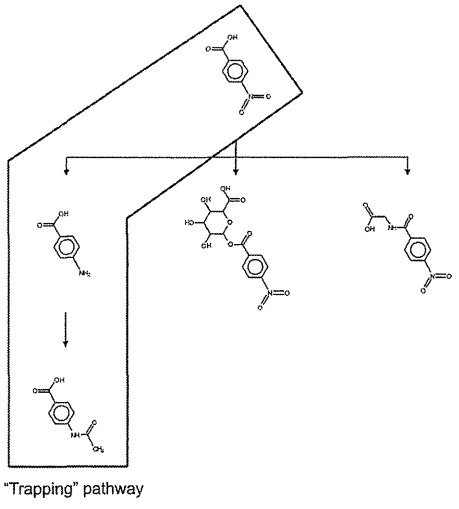

Figure 12. Simulated metabolic tree of 4-nitrobenzoic acid (62-23-7). The parent chemical and its metabolite 4-aminobenzoic acid are considered to be "trapped" in a liver detoxification pathway.

4-Nitrobenzoic acid was found to be excreted in rat urine as 4-aminobenzoic acid and its conjugates after oral and intraperitoneal administration.[76] Currently, the "false positive" chemicals are subjected to an expert analysis of their genotoxic potential; eventually, this will result in an expanded list of "trapping" detoxification pathways in liver.

SUMMARY AND CONCLUSIONS

A workflow relating genotoxicity effects at three different levels of biological organization has been constructed to facilitate

the systematic evaluation of empirical data. This required the collection of a large amount of data for in vitro mutagenicity (Ames, CA, and MLA); in vivo liver genotoxicity (UDS, Comet, and TGR); and in vivo bone marrow genotoxicity (MNT) of diverse chemicals. The database has been subjected to a critical analysis to minimize as many inconsistencies as possible between the different sources.

A number of levels of the in vitro–in vivo relationship can be derived in the workflow (as depicted in Figure 1). A first level begins with the in vitro negative (nonmutagenic) chemicals, for which two possible in vivo genotoxicity outcomes appear to be feasible. The majority of these chemicals are not expected to produce in vivo genotoxic damage neither in liver nor in the remote bone marrow (level I). However, for a small minority of the nonmutagenic chemicals, in vivo bioactivation reactions can take place to produce reactive metabolites capable to induce in vivo genotoxicity (level II). The principle organ for in vivo metabolic activation is assumed to be liver; no examples for direct bone marrow activation were identified. According to the adopted in vitro–in vivo relationship developed in this work, in vitro negative results can usually be used as sufficient evidence for a lack of in vivo genotoxicity.

The fate of in vitro positive chemicals in vivo is also described. First, because of in vivo detoxification "logic", in vitro positive chemicals could be deactivated in liver; subsequently, no in vivo MNT effect is expected in the bone marrow for these chemicals (level III). The in vivo detoxification "logic" is simulated by introducing so-called "trapping" metabolic pathways. In contrast with the in vitro-generated metabolites, which are freely available to interact with macromolecules, the metabolites in vivo are "trapped" by being engaged in enzyme complexation (channeling effects) and subsequently are unable to interact with DNA and proteins. In vitro positives would also be in vivo liver positive if parent compounds and/or metabolites are not engaged in detoxification pathways. Considering this, there are two options: in vivo liver positives could be "bioexhausted" (e.g., extremely reactive chemicals involved in off-target protein reactions approaching to the bone marrow) and thus lack in vivo MNT effects (level IV), or alternatively, the in vivo liver genotoxic chemicals are in vivo MNT positive if available at the remote target (level V).

The development of the genotoxicity workflow is based on the main assumption that any differences in vitro and in vivo for the same chemicals can be attributed to differences in their bioavailability in the organs of investigation rather than their reactivity. In other words, parent compounds and/or metabolites, which are reactive toward DNA and proteins, could have different in vitro/in vivo effects due to differences in their availability in target organs.

On the basis of the scheme, two models for in vivo genotoxicity have been developed. The models have been combined on the same platform: a new in vivo metabolism simulator explicitly describing the in vivo detoxification effects and a reactivity module based on the electrophilicity of chemicals toward DNA and proteins. Given the accuracy of experimental data (approximately 75–80%), the in vivo MNT model exhibited a reasonable performance: sensitivity of 82% and specificity of 61%.

On the other hand, the in vivo liver genotoxicity model was developed as an outcome of the relationships established in the scheme. According to these relationships, in vitro mutagenic chemicals that are not involved in "trapping" detoxification pathways are considered capable of causing DNA and/protein damage and hence in vivo liver genotoxic effects. Thus, the overall performance of the current model appears to be relatively low (sensitivity of 85% and specificity of 49%). This insufficiency is attributed to the fact that the model is indirectly derived as a result of the in vitro–in vivo gap investigation, rather than from a training set of chemicals. Hence, the current model does not claim to be complete and will require further work (which is ongoing) before it is acceptable for use. By deriving it, we rather aimed to demonstrate the feasibility of the workflow for modeling complex genotoxicity end points. Further work will be focused on collecting more experimental data and performing further in-depth analysis on the training set chemicals to rationalize their detoxification pathways. While the workflow has been derived using genotoxicity information, the approach could be potentially generalized to examine in vitro–in vivo relationships for other complex end points.

■ ASSOCIATED CONTENT

Supporting Information

Appendices I–III containing the set of chemicals and their corresponding calls in the various in vitro and in vivo liver genotoxicity and MNT tests. This material is available free of charge via the Internet at http://pubs.acs.org.

■ AUTHOR INFORMATION

Corresponding Author

*E-mail: patlewig@hotmail.com.

Funding

This work was partially funded by the Istituto Superiore di Sanita'—Swiss Federal Office of Public Health Project: "Construction of a chemical relational database on *in vivo* micronucleus assay results". MetaPath (LMC) development was partially supported by the U.S. Environmental Protection Agency (Athens, United States) under Grant CR-83199501-0. The workgroup is grateful to the L'Oreal, Dow Chemical, and DuPont companies that supplied data, expert knowledge, and partial funding to support the presenting work.

■ ABBREVIATIONS

MNT, micronucleus test; CA, chromosomal aberration; MLA, mouse lymphoma assay; UDS, unscheduled DNA synthesis; TGR, transgenic rodent gene mutation assay; TIMES, tissue metabolism simulator; QSAR, quantitative structure–activity relationship; SA, structural alerts; ADME, absorption, distribution, metabolism, excretion; *hprt*, hypoxanthine–guanine phosphoribosyltransferase

■ REFERENCES

(1) Miller, E., and Miller, J. (1981) Searches for ultimate chemical carcinogens and their reactions with cellular macromolecules. *Cancer 47*, 2327–2345.

(2) Ashby, J. (1985) Fundamental structural alerts to potential carcinogenicity or noncarcinogenicity. *Environ. Mutagen. 7*, 919–921.

(3) Ashby, J., and Tennant, R. W. (1991) Definitive relationships among chemical structure, carcinogenicity and mutagenicity for 301 chemicals tested by the U.S. NTP. *Mutat. Res. 257*, 229–306.

(4) Bailey, A., Chanderbhan, N., Collaz-Braier, N., Cheeseman, M., and Twaroski, M. (2005) The use of structural-activity relationship analysis in the food contact notification program. *Regul. Toxicol. Pharmacol. 42*, 225–235.

(5) Kazius, J., McGuire, R., and Bursi, R. (2005) Derivation and validation of toxicophores for mutagenicity prediction. *J. Med. Chem. 48*, 312–320.

(6) Mekenyan, O., Dimitrov, S., Serafimova, R., Thompson, E., Kotov, S., Dimitrova, N., and Walker, J. (2004) Identification of the structural requirements for mutagenicity by incorporating molecular flexibility and metabolic activation of chemicals I: TA 100model. *Chem. Res. Toxicol. 17*, 753–766.

(7) Woo, Y. T., and Lai, D. Y. (2003) Mechanisms of action of chemical carcinogens, and their role in structure-activity relationship (SAR) analysis and risk assessment. In *Quantitative Structure–Activity Relationship (QSAR) Models of Mutagens and Carcinogens* (Benigni, R., Ed.) pp 41–80, CRC Press, Boca Raton.

(8) Benigni, R., and Bossa, C. (2008) Structural alerts for carcinogenicity, and the Salmonella assay system: A novel insight through the chemical relational databases technology. *Mutat. Res. 659*, 248–261.

(9) Chung, K. T., Kirkovsky, L., Kirkovski, A., and Purcell, W. P. (1997) Review of mutagenicity of monocyclic aromatic amines: quantitative structure-activity relationships. *Mutat. Res. 387*, 1–16.

(10) Benigni, R., Netzeva, T. I., Benfenati, E., Bossa, C., Franke, R., Helma, C., Hulzebos, E., Marchant, C., Richard, A., Woo, Y.-T., and Yang, C. (2007) The expanding role of predictive toxicology: An update on the (Q)SAR models for mutagens and carcinogens. *J. Environ. Sci. Health, Part C 25*, 53–97.

(11) Serafimova, R., Gatnik, M. F., and Worth, A. (2010) Review of QSAR Models and software tools for predicting genotoxicity and carcinogenicity. *JRC Scientific and Technical Reports*, http://publications.jrc.ec.europa.eu/repository/handle/111111111/14330.

(12) Serafimova, R., Todorov, M., Pavlov, T., Kotov, S., Jacob, E., Aptula, A., and Mekenyan, O. (2007) Identification of the structural requirements for mutagencitiy by incorporating molecular flexibility and metabolic activation of chemicals. II. General Ames mutagenicity model. *Chem. Res. Toxicol. 20*, 662–676.

(13) Mekenyan, O., Todorov, M., Serafimova, R., Stoeva, S., Aptula, A., Finking, R., and Jacob, E. (2007) Identifying the structural requirements for chromosomal aberration by incorporating molecular flexibility and metabolic activation of chemicals. *Chem. Res. Toxicol. 20*, 1927–1941.

(14) Benigni, R., Bossa, C., and Worth, A. (2010) Structural analysis and predictive value of the rodent *in vivo* micronucleus assay results. *Mutagenesis 25*, 335–341.

(15) ECHA (2008) Guidance on information requirements and chemical safety assessment Chapter R.7a: Endpoint specific guidance (see http://guidance.echa.europa.eu/docs/guidance_document/information_requirements_r7a_en.pdf?vers=02_02_10).

(16) Krishna, G., and Hayashi, M. (2000) *In vivo* rodent micronucleus assay: Protocol, conduct and data interpretation. *Mutat. Res. 455*, 155–166.

(17) Wang, J., Sawyer, J. R., Chen, L., Chen, T., Honma, M., Mei, N., and Moore, M. M. (2009) The mouse lymphoma assay detects recombination, deletion, and aneuploidy. *Toxicol. Sci. 109*, 96–105.

(18) Dertinger, S. D., Torous, D. K., Hayashi, M., and MacGregor, J. T. (2011) Flow cytometric scoring of micronucleated erythrocytes: An efficient platform for assessing *in vivo* cytogenetic damage. *Mutagenesis 26*, 139–145.

(19) Kirkland, D., Aardema, M., Henderson, L., and Müller, L. (2005) Evaluation of the ability of a battery of three *in vitro* genotoxicity tests to discriminate rodent carcinogens and non-carcinogens. I. Sensitivity, specificity and relative predictivity. *Mutat. Res. 584*, 1–256.

(20) Kirkland, D., Pfuhler, S., Tweats, D., Aardema, M., Corvi, R., Darroudi, F., Elhajouji, A., Glatt, H., Hastwell, P., Hayashi, M., Kasper, P., Kirchner, S., Lynch, A., Marzin, D., Maurici, D., Meunier, J. R, Mueller, L., Nohynek, G., Parry, J., Parry, E., Thybaud, R. T., Benthem, J., Vanparys, P., and White, P. (2007) How to reduce false positive results when undertaking *in vitro* genotoxicity testing and thus avoid unnecessary follow-up animal tests: Report of an ECVAM Workshop. *Mutat. Res. 628*, 31–55.

(21) Kirkland, D., and Speit, G. (2008) Evaluation of the ability of a battery of three *in vitro* genotoxicity tests to discriminate rodent carcinogens and non-carcinogens. III. Appropriate follow-up testing *in vivo*. *Mutat. Res. 654*, 114–132.

(22) Mekenyan, O., Patlewicz, G., Dimitrova, G., Kuseva, C., Todorov, M., Stoeva, S., Kotov, S., and Donner, E. M. (2010) The use of genotoxicity information in the development of Integrated Testing Strategies (ITS) for skin sensitization. *Chem. Res. Toxicol. 23*, 1519–1540.

(23) Patlewicz, G., Mekenyan, O., Dimitrova, G., Kuseva, C., Todorov, M., Kotov, S., Stoeva, S., and Donner, E. M. (2010) Can mutagenicity information be useful in an Integrated Testing Strategy (ITS) for skin sensitisation? *SAR QSAR Environ. Res. 21*, 619–656.

(24) Mekenyan, O., Ivanov, J., Karabunarliev, S., Bradbury, S., Ankley, G., and Karcher, W. (1997) A computationally-based hazard identification algorithm that incorporates ligand flexibility. 1. Identification of potential androgen receptor ligands. *Environ. Sci. Technol. 31*, 3702–3711.

(25) Mekenyan, O. G., Nikolova, N., Schmieder, P., and Veith, G. D. (2004) COREPA-M: A Multi Dimensional Formulation of COREPA. *QSAR Comb. Sci. 23*, 5–18.

(26) Gatto, B., Capranico, G., and Palumbo, M. (1999) Drugs acting on DNA topoisomerases: Recent advances and future perspectives. *Curr. Pharm. Des. 5*, 195–215.

(27) Mekenyan, O., Dimitrov, D., Nikolova, N., and Karabunarliev, S. (1999) Conformational Coverage by a Genetic Algorithm. *Chem. Inf. Comput. Sci. 39*, 997–1016.

(28) Pavlov, T., Todorov, M., Serafimova, R., Aladjov, H., and Mekenyan, O. (2007) Conformational coverage by a genetic algorithm: Saturation of conformational space. *J. Chem. Inf. Model. 47*, 851–863.

(29) Mekenyan, O., Dimitrov, S., Pavlov, T., and Veith, G. D. (2004) A systematic approach to simulating metabolism in computational toxicology. I. The TIMES Heuristic Modelling Framework. *Curr. Pharm. Des. 10*, 1273–1293.

(30) Mekenyan, O., Dimitrov, S., Dimitrova, N., Dimitrova, G., Pavlov, T., Chankov, G., Kotov, S., Vasilev, K., and Vasilev, R. (2006) Metabolic activation of chemicals: in-silico simulation. *SAR QSAR Environ. Res. 17*, 107–120.

(31) Mekenyan, O., Nikolova, N., Karabunarliev, S., Bardbury, S., Ankley, G., and Hansen, B. (1999) New developments in a hazard identification algorithm for hormone receptor ligands. *Quant. Struct.-Act. Relat. 18*, 139–153.

(32) Tweats, D. J, Blakey, D., Heflich, R. H., Jacobs, A., Jacobsen, S. D., Morita, T., Nohmi, T., O'Donovan, M. R., Sasaki, Y. F, Sofuni, T., and Tice, R. (2007) Report of the IWGT working group on strategy/interpretation for regulatory *in vivo* tests. II. Identification of *in vivo*-only positive compounds in the bone marrow micronucleus test. *Mutat. Res. 627*, 92–105.

(33) Shiba, D. A., and Weinkam, R. J. (1983) The *in vivo* Cytotoxic Activity of Procarbazine and Procarbazine Metabolites Against L1210 Ascites Leukemia Cells in CDF1Mice and the Effects of Pretreatment with Procarbazine, Phenobarbital, Diphenylhydantoin, and Methylprednisolone upon *in vivo* Procarbazine Activity. *Cancer Chemother. Pharmacol. 11*, 124–129.

(34) Snyder, R., Witz, G., and Goldstein, B. D. (1993) The Toxicology of Benzene. *Environ. Health Perspect. 100*, 293–306.

(35) Ghanayem, B. I., and Hoffler, U. (2007) Investigation of Xenobiotics Metabolism, Genotoxicity, and Carcinogenicity Using Cyp2e1−/− Mice. *Curr. Drug Metab. 8*, 728–749.

(36) Mohtashamipur, E., Triebel, R., Straeter, K., and Norpoth, K. (1987) The bone marrow clastogenicity of eight halogenated benzenes in male NMRI mice. *Mutagenesis 2*, 111–113.

(37) Morita, T., Asano, N., Awogi, T., Sasaki, Y. F., Sato, S., Shimada, H., Sutou, S., Suzuki, T., Wakata, A., Sofuni, T., and Hayashi, M. (1997) Evaluation of the rodent micronucleus assay to screen IARC carcinogens (group 1, 2A, and2B). The summary report of the 6th collaborative study by CSGMT/JEMS. *Mutat. Res. 389*, 3–122.

(38) National Toxicology Program (1987) *Toxicology and Carcinogenesis Studies of 1,4-Dichlorobenzene (CAS No. 106-46-7) in F344/N Rats and B6C3F1Mice (Gavage Studies)*, Tech. Rep. Ser. No. 319, NIH Publ. No. 87-2575, National Toxicology Program, Research Triangle Park, NC.

(39) Tegethoff, K., Herbold, B. A., and Bomhard, E. M. (2000) Investigations on the mutagenicity of 1,4-dichlorobenzene and its main metabolite 2,5-dichlorophenol *in vivo* and *in vitro*. *Mutat. Res. 470*, 161−167.

(40) Butterworth, B. E., Aylward, L. L., and Hays, S. M. (2007) A Mechanism-Based Risk Assessment for 1,4-Dichlorobenzene. *Reg. Toxicol. Pharmacol. 49*, 138−148.

(41) Werner, S., Kunz, S., Wolff, T., and Schwartz, L. R. (1996) Steroidal Drug Cyproterone Acetate Is Activated to DNA-Binding Metabolites by Sulfonation. *Cancer Res. 56*, 4391−4397.

(42) Kasper, P. (2001) Cyproterone Acetate: A Genotoxic Carcinogen? *Pharmacol. Toxicol. 88*, 223−231.

(43) Recio, L., Hobbs, C., Caspary, W., and Witt, K. L. (2010) Dose-response assessment of four genotoxic chemicals in a combined mouse and rat micronucleus (MN) and Comet assay protocol. *J. Toxicol. Sci. 35*, 149−162.

(44) Oldham, J. W., Preston, R. F., and Paulson, J. D. (1986) Mutagenicity testing of selected analgesics in Ames *Salmonella* strains. *J. Appl. Toxicol. 6*, 237−243.

(45) Camus, A.-M., Friesen, M., Croisy, A., and Bartsch, H. (1982) Species-specific activation of phenacetin into bacterial mutagens by hamster liver enzymes and identification of *N*-hydroxyphenacetin *O*-Glucuronide as a promutagen in the urine. *Cancer Res. 42*, 3201−3208.

(46) Dearfield, K. L., McCarroll, N. E., Protzel, A., Stack, H. F., Jackson, M. A., and Waters, M. D. (1999) A survey of EPA/OPP and open literature on selected pesticides chemicals II. Mutagenicity and carcinogenicity of selected chloroacetanilides and related compounds. *Mutat. Res. 443* (1−2), 183−221.

(47) Hinson, J. A. (1983) Reactive metabolites of phenacetin and acetaminophen: A review. *Environ. Health Perspect. 49*, 71−79.

(48) Sekihashi, K., Sasaki, T., Yamamoto, A., Kawamura, K., Ikka, T., Tsuda, S., and Sasaki, Y. F. (2001) A comparison of intraperitoneal and oral gavage administration in comet assay in mouse eight organs. *Mutat. Res. 493*, 39−54.

(49) Takasawa, H., Suzuki, H., Ogawa, I., Shimada, Y., Kobayashi, K., Terashima, Y., Matsumoto, H., Aruga, C., Oshida, K., Ohta, R., Imamura, T., Miyazaki, A., Kawabata, M., Minowa, S., and Hayashi, M. (2010) Evaluation of a liver micronucleus assay in young rats (III): A study using nine hepatotoxicants by the Collaborative Study Group for the Micronucleus Test (CSGMT)/Japanese Environmental Mutagen Society (JEMS)—Mammalian Mutagenicity Study Group (MMS). *Mutat. Res. 698*, 30−37.

(50) Wakata, A., Miyamae, Y., Sato, S., Suzuki, T., Morita, T., Asano, N., Awogi, T., Kondo, K., and Hayashi, M. (1998) Evaluation of the rat micronucleus test with bone marrow and peripheral blood: Summary of the 9th collaborative study by CSGMT/JEMS—MMS. *Environ. Mol. Mutagen. 32*, 84−100.

(51) CSGMT (Collaborative Study Group for the Micronucleus Test) (1992) Micronucleus test with mouse peripheral blood erythrocytes by acridine orange supravital staining: The summary report of the 5th collaborative study by CSGMT/JEMS—MMS. *Mutat. Res. 278*, 83−98.

(52) WHO (1984) Epichlorohydrin. *Environmental Health Criteria 33*, International Programme on Chemical Safety, WHO, Geneva; http://www.bvsde.ops-oms.org/bvsacg/e/cd-cagua/guias/b.parametos/4.BasTox/IPCS/059.epichlorohydrin.pdf.

(53) Benigni, R., Bossa, C., Tcheremenskaia, O., and Worth, A. (2009) Development of Structural Alerts for the *in vivo* Micronucleus Assay in Rodents. *JRC Scientific and Technical Reports, EUR 23844 EN—2009*, 1−42.

(54) Wirnitzer, U. (2005) 4-Amino-2-Hydroxytoluene (WR 23032)—Comet Assay in vivo in liver, stomach and urinary bladder epithelium male rat, Bayer AG, as cited in Opinion on Scientific Committee on Consumer Products (SCCP) on 4-Amino-2-hydroxytoluene. COLIPA No. A27, 9th plenary meeting of 10 October 2006.

(55) Witt, K., Livanos, E., Kissling, G., Torous, D., Caspary, W., Tice, R., and Recio, L. (2008) Comparison of flow cytometry- and microscopy-based methods for measuring micronucleated reticulocyte frequencies in rodents treated with nongenotoxic and genotoxic chemicals. *Mutat. Res. 649*, 101−113.

(56) Hedtke, B., Gao, Z., Chen, L., Weber, W., and Dix, K. (2008) Metabolism and Disposition of 5-Amino o-Cresol in Female F344 Rats and B6C3F1Mice. *Xenobiotica 38*, 171−184.

(57) Dimitrov, S., Dimitrova, G., Pavlov, T., Dimitrova, N., Patlewicz, G., Niemela, J., and Mekenyan, O. (2005) A Stepwise Approach for Defining the Applicability Domain of SAR and QSAR Models. *J. Chem. Inf. Model. 45*, 839−849.

(58) Brambilla, G., and Martelli, A. (2004) Failure of the Standard Battery of Short-Term Tests in Detecting Some Rodent and Human Genotoxic Carcinogens. *Toxicology 196*, 1−19.

(59) NTP Technical Report on the Toxicity Studies of 1,1,1-trichloroethane, NTP TR 41, 2000; http://ntp.niehs.nih.gov/ntp/htdocs/ST_rpts/tox041.pdf.

(60) Sala, M., Gu, Z. G., Moens, G., and Chouroulinkov, I. (1982) *In vivo* and *In vitro* Biological Effects of the flame Retardants Tris (2,3-dibromopropyl) phosphate and Tris(2-chloroethyl)orthophosphate. *Eur. J. Cancer Clin. Oncol. 18* (12), 1337−1344.

(61) Hardy, M. L. (2002) The toxicology of the three commercial polybrominated diphenyl oxide (ether) flame retardants. *Chemosphere 46*, 757−777.

(62) Busk, L., Sjoestroem, B., and Ahlborg, U. G. (1984) Effects of vitamin A on cyclophosphamide mutagenicity *in vitro* (Ames test) and *in vivo* (mouse micronucleus test). *Food Chem. Toxicol. 22*, 725−730.

(63) Acetanilide, SIDS Initial Assessment Report for 13th SIAM, Bern, November 2001.

(64) Pool-Zobel, B. L., Guigas, C., Klein, R., Neudecker, C., Renner, H. W., and Schmezer, P. (1993) Assessment of genotoxic effects by lindane. *Food Chem. Toxicol. 31*, 271−283.

(65) Charles, J. M., Cunny, H. C., Wilson, R. D., Ivett, J. L., Murli, H., Bus, J. S., and Gollapudi, B. (1999) *In vivo* micronucleus assays on 2,4-dichlorophenoxyacetic acid and its derivatives. *Mutat. Res. 444* (1), 227−234.

(66) Committee for Veterinary Medical Products, Coumafos, Summary Report, January 1999, The European Agency for Evaluation of Medicinal Products, Veterinary Medicines Evaluation Unit.

(67) Guan, X., Davis, M. R., Tang, C., Jochheim, C. M., Jin, L., and Baillie, T. A. (1999) Identification of S-(n-butylcarbamoyl)glutathione, a reactive carbamoylating metabolite of tolbutamide in the rat, and the evaluation of its inhibitory effects on the glutathione reductase *in vitro*. *Chem. Res. Toxicol. 12*, 1138−1143.

(68) Buckley, L. A., Coleman, D. P., Burgess, J. P., Thomas, B. F., Burka, L. T., and Jeffcoat, A. R. (1999) Identification of urinary metabolites of isoprene in rats and comparison with mouse urinary metabolites. *Drug Metab. Dispos. 27* (7), 848−854.

(69) Gervasi, P. G., and Longo, V. (1990) Metabolism and mutagenicity of isoprene. *Environ. Health Perspect. 86*, 85−87.

(70) Claxton, L. D., Matthews, P. P., and Warren, S. H. (2004) The genotoxicity of ambient outdoor air, a review: Salmonella mutagenicity. *Mutat. Res. 567* (2−3), 347−399.

(71) Hakura, A., Mochida, H., Tsutsui, Y., and Yamatsu, K. (1995) Mutagenicity of benzoquinones for Salmonella tester strains. *Mutat. Res. 347*, 37−43.

(72) Hissink, A. M., Oudshoorn, M. J., Van Ommen, B., and Van Bladeren, P J. (1997) Species and strain differences in the hepatic cytochrome P450-mediated biotransformation of 1,4-dichlorobenzene. *Toxicol. Appl. Pharmacol. 145*, 1−9.

(73) Rietjens, I. M. C. M., den Besten, C., Hanzlik, R. P., and van Bladeren, P. J. (1997) Cytochrome P450-catalyzed oxidation of halobenzene derivatives. *Chem. Res. Toxicol. 10*, 629−635.

(74) den Besten, C., Smink, M. C. C., de Vries, E. J., and van Bladeren, P. J. (1991) Metabolic activation of 1,2,4-trichlorobenzene and pentachlorobenzene by rat liver microsomes: A major role for quinone metabolites. *Toxicol. Appl. Pharmacol. 108*, 223−233.

(75) Furuya, K. N., Durie, P. R, Roberts, E. A., and Soldin, S. J. (1995) Glycine Conjugation of Para-Aminobenzoic Acid (PABA): A Quantitative Test of Liver Function. *Clin. Biochem. 28*, 531−540.

1421 (76) Gardner, D. M., and Renwick, A. G. (1978) The Reduction of
1422 Nitrobenzoic Acid in the Rat. *Xenobiotica 8*, 679–690.
1423 (77) Sawatari, K., Nakanishi, Y., and Matsushima, T. (2001)
1424 Relationships between Chemical Structures and Mutagenicity: A
1425 Preliminary Survey for a Database of Mutagenicity Test Results of
1426 New Work Place Chemicals. *Ind. Health 39*, 341–345.
1427 (78) International Agency for Research on Cancer (IARC) (1987)
1428 *IARC Monographs on the Evaluation of the Carcinogenic Risk of*
1429 *Chemicals to Humans—Views and Expert Opinions of an IARC Working*
1430 *Group*, IARC, Lyon, France (Russian ed.).
1431 (79) Kovacic, P., and Jacintho, J. D. (2001) Mechanisms of carcino-
1432 genesis: Focus on oxidative stress and electron transfer. *Curr. Med.*
1433 *Chem. 8*, 773–796.
1434 (80) Freidig, A. P., Verhaar, H. J. M., and Hermens, J. L. M. (1999)
1435 Quantitative structure property relationships for the chemical reactivity
1436 of actylates and methacrylates. *Environ. Toxicol. Chem. 18*, 1133–1139.
1437 (81) Metz, B., Kersten, G. F. A., Hoogerhout, P., Brugghe, H. F.,
1438 Timmermans, H. A. M., de Jong, A., Meiring, H., ten Hove, J.,
1439 Hennink, W. E., Crommelin, D. J. A., and Jiskoot, W. (2004) Iden-
1440 tification of formaldehyde-induced modifications in proteins. *J. Biol.*
1441 *Chem. 279*, 6235–6243.

dx.doi.org/10.1021/tx200547s | *Chem. Res. Toxicol.* XXXX, XXX, XXX–XXX

Mutagenesis vol. 28 no. 1 pp. 81–88, 2013
Advance Access publication 17 October 2012

doi:10.1093/mutage/ges056

Miscoding properties of 8-chloro-2′-deoxyguanosine, a hypochlorous acid-induced DNA adduct, catalysed by human DNA polymerases

Akira Sassa,[1,2], Nagisa Kamoshita[1], Tomonari Matsuda[3], Yuji Ishii[4], Isao Kuraoka[5], Takehiko Nohmi[1], Toshihiro Ohta[2], Masamitsu Honma[1] and Manabu Yasui[1,*]

[1]Division of Genetics and Mutagenesis, National Institute of Health Sciences, Setagaya-ku, Tokyo 158–8501, Japan, [2]School of Life Sciences, Tokyo University of Pharmacy and Life Sciences, Hachiouji-shi, Tokyo 192–0392, Japan, [3]Research Center for Environmental Quality Management, Kyoto University, Otsu, Shiga 520–0811, Japan, [4]Division of Pathology, National Institute of Health Sciences, Setagaya-ku, Tokyo 158–8501, Japan, [5]Graduate School of Engineering Science, Osaka University, Toyonaka, Osaka 560–8531, Japan.

*To whom correspondence should be addressed. Tel: +81-3-3700-1141 (ex. 434); Fax: +81-3-3700-2348; Email: m-yasui@nihs.go.jp

Received on June 15, 2012; revised on July 14, 2012; accepted on August 3, 2012

Many chronic inflammatory conditions are associated with an increased risk of cancer development. At the site of inflammation, cellular DNA is damaged by hypochlorous acid (HOCl), a potent oxidant generated by myeloperoxidase. 8-Chloro-2′-deoxyguanosine (8-Cl-dG) is a major DNA adduct formed by HOCl and has been detected from the liver DNA and urine of rats administered lipopolysaccharide in an inflammation model. Thus, the 8-Cl-dG lesion may be associated with the carcinogenesis of inflamed tissues. In this study, we explored the miscoding properties of the 8-Cl-dG adduct generated by human DNA polymerases (pols). Site-specifically modified oligodeoxynucleotide containing a single 8-Cl-dG was prepared and used as a template in primer extension reactions catalysed by human pol α, κ or η. Primer extension reactions catalysed by pol α and κ in the presence of all four dNTPs were slightly retarded at the 8-Cl-dG site, while pol η readily bypassed the lesion. The fully extended products were analysed to quantify the miscoding frequency and specificity of 8-Cl-dG using two-phased polyacrylamide gel electrophoresis (PAGE). During the primer extension reaction in the presence of four dNTPs, pol κ promoted one-base deletion (6.4%), accompanied by the misincorporation of 2′-deoxyguanosine monophosphate (5.5%), dAMP (3.7%), and dTMP (3.5%) opposite the lesion. Pol α and η, on the other hand, exclusively incorporated dCMP opposite the lesion. The steady-state kinetic studies supported the results obtained from the two-phased PAGE assay. These results indicate that 8-Cl-dG is a mutagenic lesion; the miscoding frequency and specificity varies depending on the DNA polymerase used. Thus, HOCl-induced 8-Cl-dG adduct may be involved in inflammation-driven carcinogenesis.

Introduction

Chronic infection by bacteria, virus or other microbes and subsequent inflammation have been implicated as risk factors for cancer development (1–3). In tissues with inflammation, phagocytic neutrophils, monocytes and macrophages secrete the heme protein myeloperoxidase (MPO), which generates the reactive oxidants such as hypobromous acid and hypochlorous acid (HOCl) (4–8). These oxidants are important for host defense by oxidizing cellular constituents of invading microorganisms (9). Such highly reactive oxidants, however, can damage host tissues, as well as pathogens, and may lead to mutagenesis and carcinogenesis.

When neutrophils contact with a pathogen, it produces a respiratory burst characterised by intense uptake of oxygen. Most of the produced superoxide ($O_2^{\cdot-}$) is rapidly converted to hydrogen peroxide (H_2O_2) spontaneously or by superoxide dismutase (10). MPO released by neutrophils utilises H_2O_2 to oxidise chloride at plasma concentrations of halide (Cl^-, 100 mM; Br^-, 20–100 μM; I^- <1 μM), resulting in the formation of the proinflammatory oxidant HOCl [Equation (1)] (6–8).

$$Cl^- + H_2O_2 + H^+ \rightarrow HOCl + H_2O \quad (1)$$

HOCl has been recognised for the ability to kill the pathogens by its strong oxidizing potential. This cytotoxic oxidant also induces significant increase in the cellular damage reflected by lipid peroxidation (11), protein oxidation (12–14) and DNA damage (15–17). 5-Chloro-2′-deoxyuridine (5-Cl-dU) is produced by MPO system in human inflammatory tissue (18–20). The accumulation of 5-Cl-dU has been shown to cause mutations, such as T:A → C:G transition, and the sister chromatid exchange (21,22). HOCl is known to react with DNA to form 5-chloro-2′-deoxycytidine (16,23,24), which could potentially perturb epigenetic signals by mimicking 5-methylcytosine at the promoter region (25,26). 8-chloro-2′-deoxyadenosine (8-Cl-dA) and 8-chloro-2′-deoxyguanosine (8-Cl-dG) also have been identified in the reaction with HOCl (23). Recently, 8-Cl-dG has been detected from the hepatic DNA of lipopolysaccharide (LPS)-treated rats and the urine of hepatocellular carcinoma patients (27). Thus, 8-Cl-dG adduct may enhance genetic alterations, resulting in carcinogenesis at the inflammation sites.

Oligodeoxynucleotides site-specifically modified with 8-Cl-dG have been used as DNA templates for investigating the miscoding properties using bacterial DNA polymerases (pols), Klenow fragment of *E. coli* and the large fragment of DNA polymerase I of *Bacillus stearothermophilus* (28). Based on the previous report, both pols preferentially incorporated 2′-deoxycytidine monophosphate (dCMP), the correct base, opposite 8-Cl-dG; the miscoding events were investigated qualitatively by primer extension reactions in the presence of a single dNTP. No quantitative analysis, therefore, has been used for exploring miscoding events generated by 8-Cl-dG adduct using human DNA pols in the presence of all four dNTPs.

We present here the quantitative determination of miscoding specificities and frequencies occurring opposite the 8-Cl-dG lesion during *in vitro* DNA replication catalysed by human DNA pol α, κ and η using a two-phased gel electrophoresis methodology that can quantify base substitutions and deletions (29–31). Pol α is essential for chromosomal replication in human tissues. Pol κ and η are involved in potentially mutagenic translesion synthesis of various DNA adducts (32–37). which may be strongly associated to mutagenesis and tumorigenesis in human cells. In addition,

steady-state kinetic analyses were also performed to measure the relative bypass frequencies past the 8-Cl-dG.

Materials and methods

General

Ultrapure dNTPs were from GE Healthcare Corp. Exonuclease-free Klenow fragment and *Eco*RI restriction endonuclease were purchased from New England Biolabs, Inc. (Ipswech, MA). 2′-Deoxyguanosine-5′-triphosphate (dGTP) and Blue Dextran were obtained from Sigma–Aldrich Corp. (St. Louis, MO). DNA templates, primers, AlexaFlour-546 dye (Alexa546)-labelled primers and standard markers were purchased from Japan Bio Service Corp. (Saitama, Japan). Alexa546 was conjugated at the 5′-terminus of primers and standard markers. These oligodeoxynucleotides were purified by 20% denaturing polyacrylamide gel electrophoresis (PAGE) before use. Human pol α (1200 units/mg of protein) was purchased from CHIMERx (Milwaukee, WI). Human pol κ was prepared as C-terminal truncations with 10 His-tags, as previously described (38). Human pol η was kindly provided by Drs. Chikahide Masutani and Fumio Hanaoka.

Synthesis of 8-Cl-dGTP

8-chloro-2′-deoxyguanosine-5′-triphosphate (8-Cl-dGTP) was synthesised as previously described (39). Briefly, 10 mM dGTP was reacted with 1 mM sodium hypochlorite (NaOCl) in 250 mM sodium phosphate buffer (pH 8.0) containing 20 μM nicotine at 37°C for 1 h (Figure 1a). The reaction was terminated by adding 10 mM methionine. The reaction mixture containing 8-Cl-dGTP was fractioned by high-performance liquid chromatography (HPLC) on a reversed phase SunFire C18 column (0.46 × 15 cm; Waters Corp.), eluted over 40 min at a flow rate 1.0 ml/min with a linear gradient of 50 mM triethylamine acetate (pH 7.0) containing 0–15% acetonitrile. Separation and purification were performed by using HPLC LC-20AB pump, SPD-M20A photodiode array detector and CBM-20A system control unit (Shimadzu Corp., Kyoto, Japan).

Enzymatic preparation of 8-Cl-dG-modified oligodeoxynucleotide

The modified 38-mer template (5′CATGCTGATGAATTCCTTCXCTTCTTT CCTCTCCCTTT, X = 8-Cl-dG) containing a single 8-Cl-dG was prepared by enzymatic incorporation of 8-Cl-dGTP using a 19-mer oligodeoxynucleotide (5′CATGCTGATGAATTCCTTC) and exonuclease-free Klenow fragment followed by ligation to an 18-mer (5′CTTCTTTCCTCTCCCTTT) with T4 DNA ligase (Figure 2), as described in our previous work (40).

Briefly, to prepare a 20-mer (5′CATGCTGATGAATTCCTTCX, X = 8-Cl-dG) containing 8-Cl-dG at the 3′-terminus, 8-Cl-dGTP (20 μM) was put into the reaction mixture that contains an unlabelled or Alexa546-labelled 19-mer primer (250 ng,5′CATGCTGATGAATTCCTTC), a 38-mer template (500 ng, 5′AAAGGGAGAGGAAAGAAZCGAAGGAATTCATCAGCATG, Z = AP-site), and exonuclease-free Klenow fragment (10 units) in 20 μl of 1× NEBuffer 2 [10 mM Tris–HCl (pH 7.9), containing 50 mM NaCl, 10 mM $MgCl_2$ and 1 mM dithiothreitol (DTT)]. After the incubation at 25°C for 1 h, the reaction was stopped by heating the sample to 75°C for 10 min. The AP-site neighbouring dCMP:8-Cl-2′-deoxycytidine monophosphate (dGMP) base site inhibited >2-mer extension by 8-Cl-dGTP incorporation at the 3′-turminus of primer (Figure 3a). We subjected the reaction sample to 20% denaturing PAGE (30 × 40 × 0.05 cm) containing 7 M urea and recovered the 8-Cl-dG-incorporated 20-mer from gel. The purified 8-Cl-dG-modified 20-mer was ligated with 5′-phosphorylated 18-mer (2 μg, 5′CTTCTTTCCTCTCCCTTT) at 4°C overnight using T4 DNA ligase (1400 units) (Takara Bio, Inc., Shiga, Japan), 0.1 mM Adenosine triphosphate (ATP) and a 24-mer template (3 μg, 5′AGGAAAGAAGCGAAGGAATTCATC) in 50 μl of 66 mM Tris–HCl (pH 7.6) containing 6.6 mM $MgCl_2$ and 10 mM DTT. The resultant 8-Cl-dG 38-mer was also purified by using 20% denaturing PAGE (Figure 2).

Liquid chromatography tandem mass spectrometry analysis of oligodeoxynucleotides

Liquid chromatography tandem mass spectrometry (LC-MS/MS) analyses were performed using a Quattro Ultima triple stage quadrupole MS (Waters-Micromass, Manchester, UK). Full-scan mode with the range of *m/z* 400-800 was conducted to monitor multicharged ion of the oligonucleotide. The oligonucleotides were dissolved with 50% methanol (approximately 6 μg/ml) and infused into mass spectrometer by using syringe pump at the flow rate of 600 μl/min. MS analyses were carried out in negative ion mode with nitrogen as the nebulizing gas. The ion source temperature was 100°C, the desolvation gas temperature was 200°C and the cone voltage was operated at a constant 35 V. Nitrogen gas was also used as the desolvation gas (700 l/h) and cone gas (35 l/h).

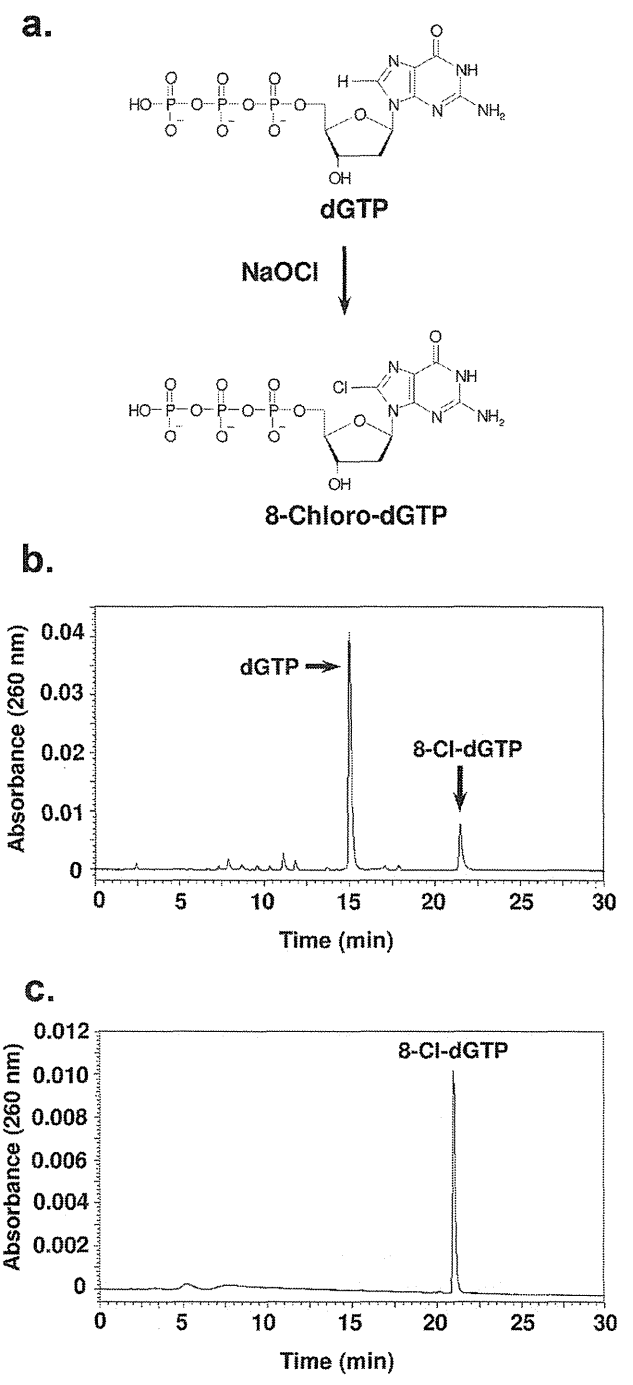

Fig. 1. Formation of 8-Cl-dGTP. (a) Synthesis of 8-Cl-dGTP. dGTP was reacted with NaOCl in the presence of nicotine in sodium phosphate buffer (pH 8.0) as described in Materials and methods. (b) HPLC separation of 8-Cl-dGTP. (c) HPLC analysis of purified 8-Cl-dGTP. 8-Cl-dGTP was isolated from dGTP on a reversed phase SunFire C18 column (0.46 × 25 cm; Waters) using a linear gradient of 50 mM triethylamine acetate (pH 7.0) containing 0–15% acetonitrile over 40 min at a flow rate 1.0 ml/min.

Enzymatic digestion of oligodeoxynucleotides

A 20-mer oligodeoxynucleotide-containing 8-Cl-dG at the 3′-terminus was incubated at 37°C for 2 h in 100 μl of 30 mM sodium acetate (pH 7.0) containing 1 mM zinc sulphate, P1 nuclease (8 units) (Wako Pure Chemical Industries, Ltd, Osaka, Japan) and *E. coli* alkaline phosphatase (5 units) (Sigma–Aldrich Corp.). Then 20 μl of 0.5 M Tris–HCl (pH 8.5) was added

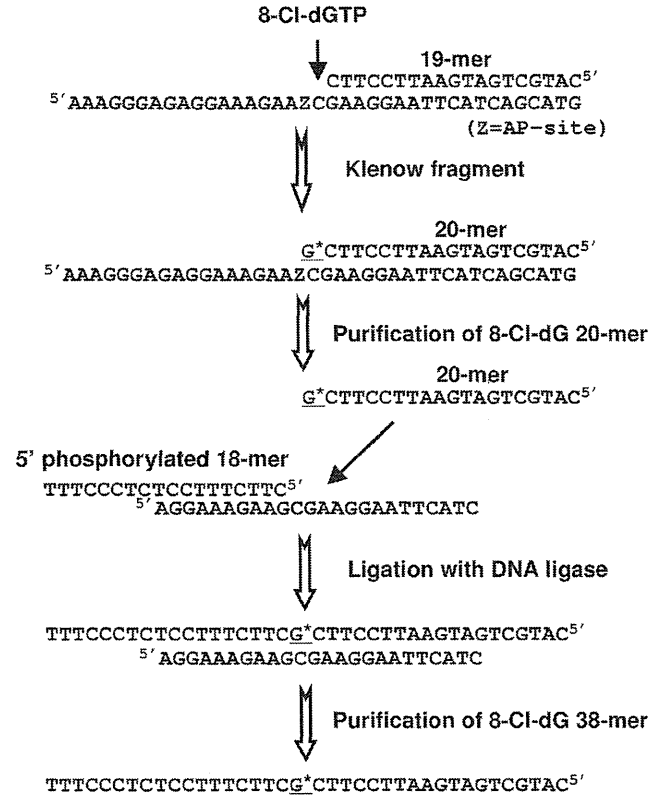

Fig. 2. Diagram of enzymatic preparation of 8-Cl-dG-modified 38-mer oligodeoxynucleotide.

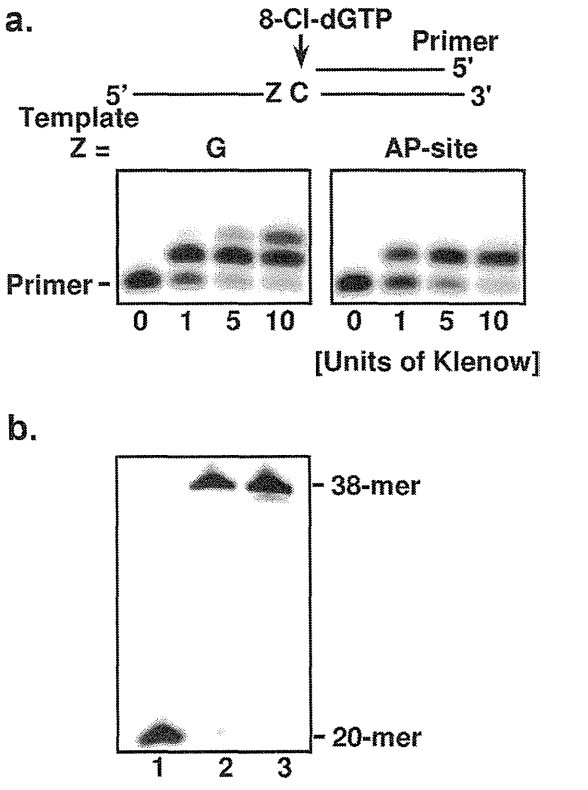

Fig. 3. Preparation of 8-Cl-dG-modified oligodeoxynucleotide. (a) Incorporation of 8-Cl-dGTP by exonuclease-free Klenow fragment (0, 1, 5 or 10 units) on without (left) and with (right) AP-site on the templates. Accumulation of 1-mer-extended 20-mer containing 8-Cl-dGMP at the 3′-terminus was observed on AP-site-introduced templates. The AP-site inhibited >2-mer extension by 8-Cl-dGTP incorporation at the 3′-turminus of the primer, resulting in the efficient recovery of 8-Cl-dG-modified 20-mer. (b) Ligation of 8-Cl-dG-modified 20-mer with 18-mer. Alexa546-labelled 20-mer-containing 8-Cl-dG was ligated with 5′-phosphorylated 18-mer at 4°C overnight using T4 DNA ligase (1400 units). The reaction mixture was analysed by 20% denaturing PAGE. Lane 1, 8-Cl-dG-modified 20-mer; lane 2, ligation product of 8-Cl-dG-modified substrate; lane 3, 38-mer standard.

to the reaction mixture and further incubated at 37°C for 2 h. The mixture was evaporated to dryness, and the resultant deoxynucleosides were extracted three times each with 100 µl of ethanol. Ethanol extracts were evaporated to dryness, dissolved in distilled water and analysed by HPLC, using COSMOSIL 5C18-MS-II column (0.46 × 25 cm; Nacalai Tesque, Inc., Kyoto). Elution was carried out using a linear gradient of 50 mM triethylamine acetate (pH 7.0) containing 0–16% acetonitrile over 40 min at a flow rate of 1.0 ml/min.

Primer extension reactions

Primer extension reactions catalysed by pol α, κ and η were conducted at 25°C for 30 min in a buffer (10 µl) containing all four dNTPs (100 µM each), using 8-Cl-dG-modified and unmodified 38-mer templates (750 fmol) primed with an Alexa546-labelled 10-mer (500 fmol, 5′AGAGGAAAGA) (Figure 5). The reaction buffer for pol α contains 40 mM Tris–HCl (pH 8.0), 5 mM $MgCl_2$, 60 mM KCl, 10 mM DTT, 250 µg/ml bovine serum albumin (BSA), and 2.5% glycerol. The reaction buffer for pol η and κ contains 40 mM Tris–HCl (pH 8.0), 5 mM $MgCl_2$, 10 mM DTT, 250 µg/ml BSA, 60 mM KCl and 2.5% glycerol. Reaction was stopped by addition of 2 µl of formamide dye containing Blue Dextran (100 mg/ml) and ethylenediaminetetraacetic acid (50 mM) and incubation at 95°C for 3 min. The whole amount of the reaction sample was subjected to 20% denaturing PAGE (30 × 40 × 0.05 cm). The separated products were visualised by using Molecular Imager FX Pro and Quantity One software (BioRad Laboratories).

Quantitation of miscoding specificities and frequencies

Using the 8-Cl-dG-modified and unmodified 38-mer oligodeoxynucleotide (750 fmol) primed with an Alexa546-labelled 10-mer (500 fmol, 5′AGAGGAAAGA), we conducted primer extension reactions catalysed by pol α (2000 fmol), κ (50 fmol) or η (50 fmol) at 25°C for 30 min in a buffer (10 µl) containing all four dNTPs (100 µM each) and subjected them to 20% denaturing PAGE (30 × 40 × 0.05 cm) (Figure 5). We used the amount of these pols so that fully extended products (approximately 28–34 mer) were 70–90% of the starting primer in primer extension reactions. The fully extended products were extracted from the gel. The recovered oligodeoxynucleotides were annealed with the unmodified 38-mer, cleaved with *Eco*RI and subjected to two-phased PAGE (20 × 65 × 0.05 cm) containing 7 M urea in the upper phase and no urea in the middle and bottom phases (each phase containing 18, 20 and 24% polyacrylamide, respectively). The phase width is approximately 10, 37 and 18 cm from the upper phase. To quantify base substitutions and deletions, we compared the mobility of the reaction products with those of Alexa546-labelled 18-mer standards containing dC, dA, dG or dT opposite the lesion and one- (Δ^1) or two-base (Δ^2) deletions (Figure 5) (29–31). The separated products were visualised by Molecular Imager FX Pro, and the bands were quantified by using Quantity One software (BioRad Laboratories). The percentage of 2′-deoxynucleoside monophosphate (dNMP) incorporation was normalised to the amount of the starting primer.

Steady-state kinetic studies of nucleotide insertion and extension

Kinetic parameters associated with nucleotide insertion opposite the 8-Cl-dG lesion and chain extension from 3′ primer terminus were determined at 25°C, using varying amounts of single dNTPs. For insertion kinetics, reaction mixtures containing dNTP (0–1000 µM) and pol κ (7–20 fmol) were incubated at 25°C for 0.5–3 min in 10 µl of Tris–HCl buffer (pH 8.0), using a 38-mer template (750 fmol) primed with an Alexa546-labelled 12-mer (500 fmol; 5′AGAGGAAAGAAG). To measure chain extension, reaction mixtures containing a 38-mer template (750 fmol) primed with an Alexa546-labelled 13-mer (500 fmol; 5′AGAGGAAAGAAGN, where N is C, A, G or T), with varying amounts of dGTP (0–500 µM) and pol κ (10 fmol) were incubated at 25°C for 0.5–2 min. The reaction samples were subjected to 20% denaturing

PAGE (30 × 40 × 0.05 cm). The Michaelis contents (K_m) and maximum rates of reaction (V_{max}) were determined by Enzyme Kinetics Module 1.1 of SigmaPlot 2001 software (SPSS, Inc.). Frequencies of dNTP insertion (F_{ins}) and chain extension (F_{ext}) were determined relative to the dC:dG base pair according to the following equation: (41,42)

$$F = (V_{max}/K_m)_{[\text{wrong pair}]}/(V_{max}/K_m)_{[\text{correct pair = dC:dG}]}.$$

Results

Enzymatic preparation of site-specifically modified oligodeoxynucleotide containing a single 8-Cl-dG

dGTP was incubated with NaOCl in phosphate buffer and then subjected to HPLC. 8-Cl-dGTP was efficiently formed and completely isolated from dGTP (Figure 1b). The retention time of 8-Cl-dGTP (21.3 min) was longer than that of dGTP (14.8 min). We purified twice the fraction of 8-Cl-dGTP (Figure 1c) and characterised it by LC–MS scanning the molecular ion peak of 8-Cl-dGTP (*m/z* 539.5). The 8-Cl-dG-modified 20-mer oligodeoxynucleotide was prepared by enzymatic incorporation of 8-Cl-dGTP by exonuclease-free Klenow fragment (Figure 3a), as described in Materials and methods. The 8-Cl-dG-modified and unmodified 20-mers were digested with P1 nuclease and alkaline phosphatase, and the resultant product was subjected to HPLC (Figure 4). The obtained molar ratio was consistent with the theoretical value of the nucleoside composition (dC:dA:dG:dT:8-Cl-dG = 5:4:3:7:1) of the 20-mer. Furthermore, the 8-Cl-dG-modified 20-mer (molecular weight 6117.4) was characterised by using LC–MS/MS analysis (Supplementary Figure S1 is available at *Mutagenesis* Online). The characterised 8-Cl-dG-modified 20-mer was ligated with 5′-phosphorylated 18-mer as described in Materials and methods. Most of the 8-Cl-dG-modified 20-mer was ligated with the 18-mer (Figure 3b, lane 2), resulting in the formation of 38-mer containing 8-Cl-dG adduct. The 8-Cl-dG-modified 38-mer was purified from the 20% denaturing PAGE.

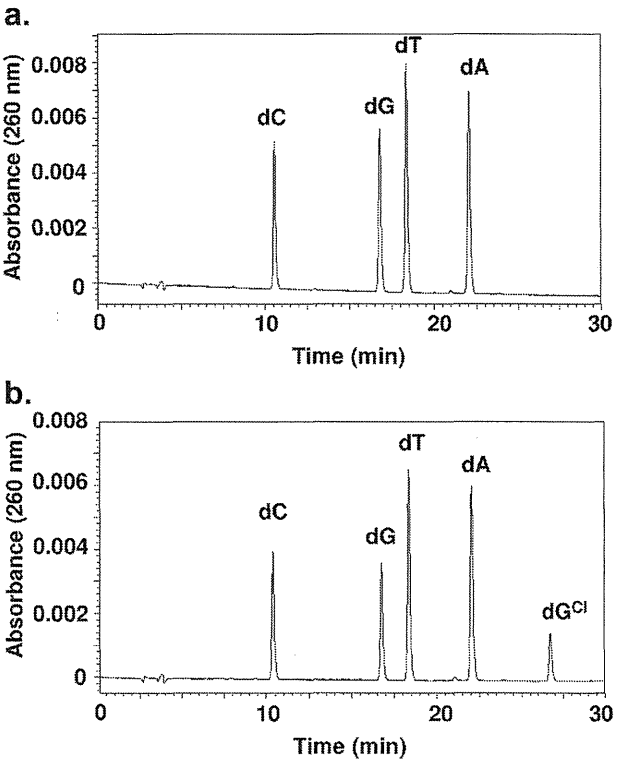

Fig. 4. HPLC elution profiles of enzymatic digests of unmodified and 8-Cl-dG-modified 20-mer. Three micrograms of unmodified (a) or 8-Cl-dG-modified (b) 20-mer (5′CATGCTGATGAATTCCTTCX, X = dG or 8-Cl-dG) was digested to nucleosides as described in Materials and methods. Ethanol extracts of the digested samples were evaporated to dryness and placed on a COSMOSIL 5C18-MS-II column (0.46 × 25 cm; Nacalai Tesque Inc., Kyoto). Elution was carried out using a linear gradient of 50 mM triethylamine acetate (pH 7.0) containing 0–16% acetonitrile over 40 min at a flow rate of 1.0 ml/min.

Primer extension reactions catalysed by human DNA pols on 8-Cl-dG-modified DNA template

Primer extension reactions were carried out using 8-Cl-dG-modified 38-mer templates in the presence of all four dNTPs and varying amounts of pol α, κ and η (Figure 5). As shown in Figure 6, the primer extension on the unmodified dG template rapidly occurred to form fully extended products by pol α, κ and η. When the 8-Cl-dG-modified template was used, the primer extension reactions catalysed by pol α and κ were slightly retarded prior to and opposite the lesion (Figure 6a and 6b). Pol η easily bypassed the 8-Cl-dG as efficiently as unmodified dG (Figure 6c). Blunt-end addition to the fully extended product (33–34 mers) was observed in all primer extension reactions, as reported earlier for *E.coli* and mammalian DNA pols (43,44).

Miscoding specificities of 8-Cl-dG adduct

Translesion synthesis catalysed by pol α, κ and η was conducted in the presence of all four dNTPs. The fully extended products (approximately 28–34-mers) past 8-Cl-dG lesion site were recovered from gel, digested by *Eco*RI and subjected to two-phased PAGE for quantitative analysis of base substitutions and deletions, as described in Materials and methods. A standard mixture of six Alexa546-labelled oligomers containing dC, dA, dG or dT opposite the lesion or one- and two-base deletions can be resolved by this method (Figure 5). When unmodified dG template was used, the incorporation of dCMP, the correct base, was observed opposite dG at 72.8%, 76.8% and 67.3% of the starting primers for pol α, κ and η, respectively (Figure 7). Using 8-Cl-dG-modified template, pol κ incorporated dCMP (63.6%) as the primary product opposite the 8-Cl-dG. Moreover, pol κ promoted one-base deletion (6.4%), associated with dGMP (5.5%), dAMP (3.7%) and dTMP (3.5%) misincorporations opposite the lesion (Figure 7b). Pol α and η exclusively incorporated dCMP opposite 8-Cl-dG lesion (Figure 7a and 7C). Small amounts of unknown products were also detected in the extension by pol η on both dG-unmodified and modified templates (arrowheads in Figure 7c). The migration of these unknown products differed from those of standard markers, implying that pol η might misinsert nucleotide on undamaged bases other than the position of the adduct site, as reported previously (45).

Steady-state kinetic studies on 8-Cl-dG-modified DNA template

Using steady-state kinetic methods, the frequency of dNTP incorporation (F_{ins}) opposite 8-Cl-dG and chain extension (F_{ext}) from the primer terminus by pol κ were measured. The F_{ins} value for dGTP (1.24×10^{-2}) was 9.7 times lower than that for dCTP (0.12), the correct base, but 2.5 and 3.7 times higher than that for dATP (5.02×10^{-3}) and dTTP (3.39×10^{-3}),

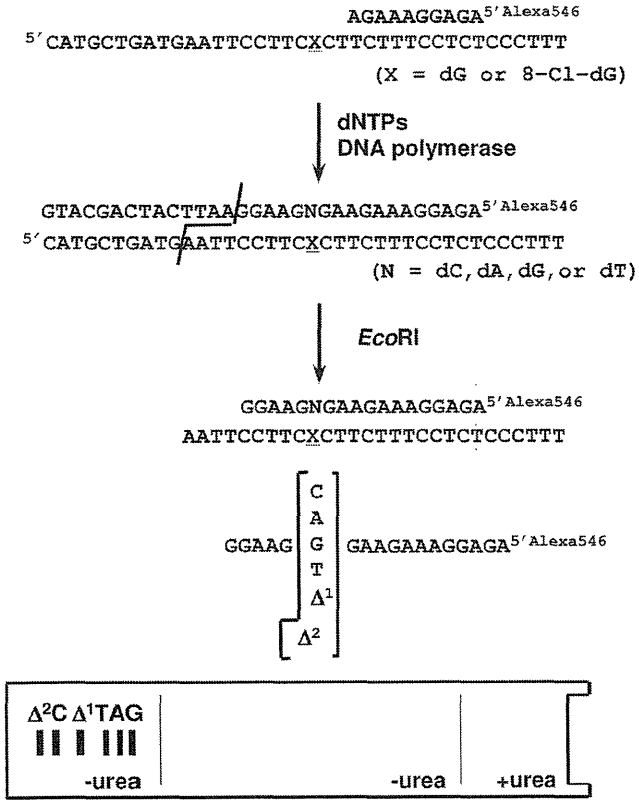

Fig. 5. Diagram of the method used to determine miscoding specificity. Unmodified and 8-Cl-dG-modified 38-mer templates were annealed to Alexa546-labelled 10-mer primer. Primer extension reactions catalysed by pol α, κ, and η were conducted in the presence of all four dNTPs. Fully extended products formed during DNA synthesis were recovered from the denaturing 20% polyacrylamide gel, annealed with the complementary 38-mer, cleaved with *Eco*RI, and subjected to two-phased PAGE. To determine miscoding specificities, mobilities of the reaction products were compared with those of 18-mer standards containing dC, dA, dG or dT opposite the lesion, and one-base- (Δ^1) or two-base (Δ^2) deletions.

respectively (Table 1). F_{ext} for dG:8-Cl-dG (2.47×10^{-3}) was 19.8 and 1.3 times lower than that for dC:8-Cl-dG (4.89×10^{-2}) and dT:8-Cl-dG (3.13×10^{-3}), but 1.4 times higher than that for dA:8-Cl-dG (1.76×10^{-3}). Therefore, the relative bypass frequency ($F_{ins} \times F_{ext}$) past the dG:8-Cl-dG pair was 192 times lower than that for dC:8-Cl-dG, but 3.5 and 2.9 times higher than that for dA:8-Cl-dG and dT:8-Cl-dG.

Discussion

Enzymatic preparation method of site-specifically modified oligodeoxynucleotide containing a single DNA adduct is a valuable tool for studying mechanisms of DNA repair and mutagenesis involving adducts (40). The conventional method for preparing such adduct-modified oligomers requires the phosphoramidite derivative of the adduct. However, it generally takes a long time to establish its synthetic method, and the number of commercially available phosphoramidites is limited. We employed the enzymatic preparation using 8-Cl-dGTP as a starting material to make modified oligomer because 8-Cl-dG phosphoramidite was also unavailable commercially. Actually, we now can purchase many types of synthetic dNTPs containing a damaged base and an analogue from chemical companies.

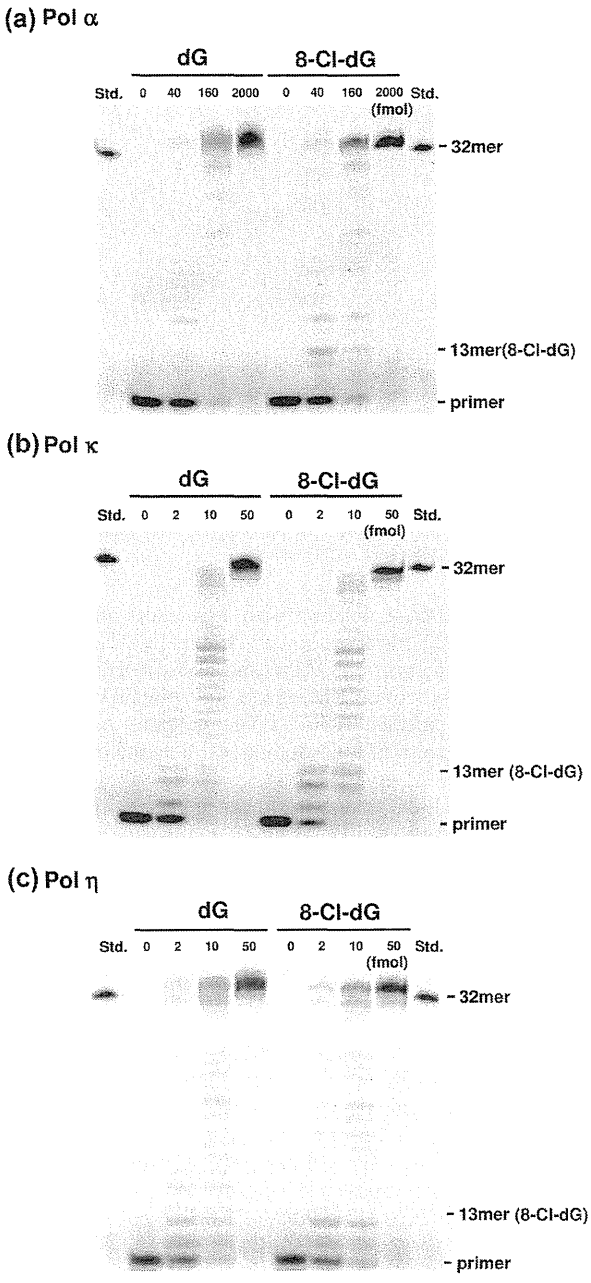

Fig. 6. Primer extension reactions catalysed by DNA polymerases on 8-Cl-dG-modified DNA templates. Unmodified and 8-Cl-dG-modified 38-mer templates were annealed to Alexa546-labelled 10-mer primer. Primer extension reactions catalysed by variable amounts (0–2000 fmol) of pol α, κ, and η were conducted at 25°C for 30 min in the presence of four dNTPs. Whole amount of the reaction mixture was subjected to 20% denaturing PAGE. 13-mer(8-Cl-dG) marks the location opposite the DNA adducts.

Thus, the enzymatic preparation method may be a useful addition to the phosphoramidite method when preparing DNA adduct-modified oligomers.

The miscoding specificities of 8-Cl-dG was determined by using an *in vitro* experimental system that can quantify base substitutions and deletions formed during the replication by pol α, κ and η in the presence of all four dNTPs (Figure 5). When pol α and η was used, both pols preferentially incorporated dCMP opposite 8-Cl-dG (Figure 7a and 7C). In contrast, pol

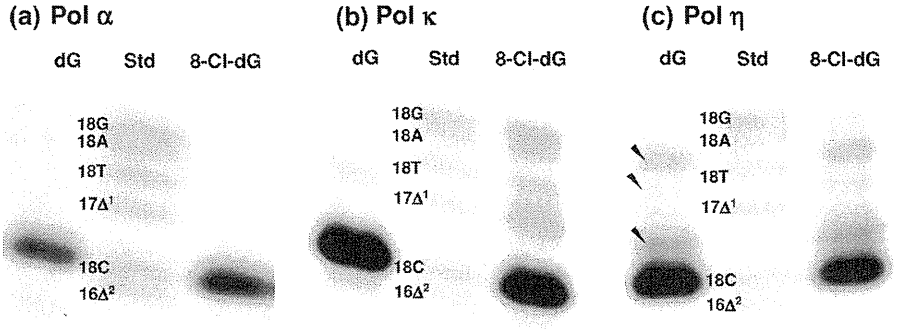

Fig. 7. Miscoding specificities of 8-Cl-dG lesion in reactions catalysed by pol α, κ, and η. Using unmodified and 8-Cl-dG-modified 38-mer templates primed with an Alexa546-labelled 10-mer, we conducted primer extension reactions at 25°C for 30 min in a buffer containing four dNTPs (100 μM each) and either pol α (2000 fmol for unmodified and 8-Cl-dG-modified templates), pol κ (50 fmol for unmodified and 8-Cl-dG-modified templates), or pol η (50 fmol for unmodified and 8-Cl-dG-modified templates), as described in Materials and methods. The extended reaction products (>28 bases long) produced on the unmodified and modified templates were extracted following 20% denaturing PAGE. The recovered oligodeoxynucleotides were annealed to the complementary unmodified 38-mer and cleaved with *Eco*RI restriction enzyme. The entire product from the unmodified and 8-Cl-dG-modified templates was subjected to two-phased PAGE (20 × 65 × 0.05 cm). Mobilities of reaction products were compared with those of 18-mer standards (Figure 5) containing dC, dA, dG or dT opposite the lesion and one-base (Δ^1) or two-base (Δ^2) deletions.

κ promoted one-base deletion with lesser amounts of dGMP, dAMP and dTMP misincorporation (Figure 7b). Thus, 8-Cl-dG can form mismatches with all wrong bases in DNA duplexes that can cause mutations. The steady-state kinetic analyses also supported these results (Table 1). This indicates that the broad miscoding spectrum of 8-Cl-dG may be generated in inflamed tissues.

Recently, 8-Cl-dG adduct has been detected in DNA from LPS-treated rat liver by LC-MS/MS analysis (27). The study showed that the relative abundance of 8-Cl-dG in hepatic DNA and urine of rat was at least 2 orders of magnitude lower than that of 8-oxo-dG. In the present study, $F_{ins} \times F_{ext}$ ratio for the dG:8-Cl-dG/dC:8-Cl-dG of pol κ was 0.0052, which is ~6200-fold lower than that for the dA:8-oxo-dG/dC:8-oxo-dG (Table 2). Overall, 8-Cl-dG is apparently less-mutagenic lesion than 8-oxo-dG.

In spite of the chemical similarity, the miscoding specificities of 8-Cl-dG were slightly different from those of 8-bromo-2′-deoxyguanosine (8-Br-dG), another major halogenated adduct (46). Pol α could bypass 8-Cl-dG in error-free manner (Figure 7a). By contrast, pol α promoted one-base deletion during the bypass of 8-Br-dG (46). Moreover, $F_{ins} \times F_{ext}$ ratio for the dG:8-Cl-dG/dC:8-Cl-dG of pol κ was 23-fold lower than that for the dG:8-Br-dG/dC:8-Br-dG (Table 2). The difference of the miscoding potential between 8-Cl-dG and 8-Br-dG may be explained by the destability effect of each halogenated base in DNA duplex. Actually, 8-Br-dG:dC base pair is less stable than 8-Cl-dG:dC in DNA duplexes as observed in the melting temperature assay (28,47). The covalent atomic radii of bromine and chlorine atoms are 114 and 99 picometre, respectively (48). The greater atomic radius of C8 atom may have more steric hindrance between the deoxyribose and C8 atom of modified guanine to destabilise dG:dC base pair, enhancing the slippage of DNA polymerases, such as one-base deletion by pol α and κ, as well as other bulky DNA adducts (49–52).

At sites of inflammation, 8-Cl-dG must be repaired by cellular DNA repair enzymes because urinary excretion of 8-Cl-dG in LPS-treated rats has been observed (27). Actually, 8-Cl-dGTP is degraded by human mutT homologue *in vitro* (39). Thus, C8-chlorinated guanine molecule in DNA may be recognised and removed by DNA repair mechanism such as base excision repair, as well as 8-oxo-dG. To investigate this possibility, we examined the incision of 8-Cl-dG paired with dC in DNA duplex by DNA glycosylases and endonucleases including human 8-oxoguanine DNA glycosylase 1 (hOGG1), endonuclease VIII-like 1 (hNEIL1), alkyladenine DNA glycosylase (hAAG), *E. coli* formamidopyrimidine DNA

Table I. Kinetic parameters for nucleotide insertion and chain extension reactions catalysed by human DNA pol κ

N:X	Insertion dNTP			Extension dGTP			$F_{ins} \times F_{ext}$
	↓GAAGAAAGGAGA			↓NGAAGAAAGGAGA			
	5′CCTTCXCTTCTTTCCTCTCCCTTT			5′CCTTCXCTTCTTTCCTCTCCCTTT			
	K_m (μM)[a]	V_{max} (%/min)[a]	F_{ins}	K_m (μM)[a]	V_{max} (%/min)[a]	F_{ext}	
C:G	9.04±2.95	8.37±1.09	1	1.63±0.16	7.82±0.40	1	1
C:X	47.8±25.3	5.10±1.16	0.12	19.1±3.84	4.48±0.39	4.89×10^{-2}	5.87×10^{-3}
A:X	409±96.2	1.90±0.20	5.02×10^{-3}	180.0±32.3	1.52±0.12	1.76×10^{-3}	8.84×10^{-6}
G:X	53.2±20.3	0.61±0.10	1.24×10^{-2}	229.3±38.3	2.72±0.21	2.47×10^{-3}	3.06×10^{-5}
T:X	1939±655	6.09±1.48	3.39×10^{-3}	115.7±15.0	1.74±0.08	3.13×10^{-3}	1.06×10^{-5}

Kinetics of nucleotide insertion and chain extension reactions were determined as described in Materials and methods. Frequencies of nucleotide insertion (F_{ins}) and chain extension (F_{ext}) were estimated by the following equation: $F = (V_{max}/K_m)_{\{wrong\ pair\}}/(V_{max}/K_m)_{\{correct\ pair = dC:dG\}}$. X = 8-Cl-dG lesion.
[a]Data were expressed as mean ± SD obtained from three independent experiments.

Table II. $F_{ins} \times F_{ext}$ past DNA adducts by human DNA pol κ

	X	8-Cl-dG (Table I)	8-oxo-dG (32)	8-Br-dG (46)
Pol κ	C:X	5.87×10^{-3}	6.21×10^{-4}	3.00×10^{-3}
	A:X	8.84×10^{-6}	$\mathbf{2.00 \times 10^{-2}}$	8.55×10^{-6}
	G:X	$\mathbf{3.06 \times 10^{-5}}$	7.65×10^{-8}	$\mathbf{3.56 \times 10^{-4}}$
	T:X	1.06×10^{-5}	5.98×10^{-5}	1.41×10^{-5}

Values in boldface indicate a primarily misincorporated base opposite the DNA adduct.

glycosylase (FPG) and endonuclease V (EndoV). Surprisingly, 8-Cl-dG is hardly cleaved by any enzymes (Supplementary Figure S2 is available at *Mutagenesis* Online). This suggests that 8-Cl-dG may be removed by the DNA repair machinery other than those DNA repair enzymes in cells. Further investigation is expected to elucidate the mechanism of repair for the inflammation-associated DNA adduct.

In conclusion, two-phased PAGE analysis and steady-state kinetic studies were performed to determine the miscoding specificities of the chlorinated DNA adduct 8-Cl-dG. 8-Cl-dG is a mutagenic lesion; the miscoding frequency and specificity varies depending on the DNA polymerase used. Thus, HOCl-induced 8-Cl-dG adduct may generate mutations at sites of inflammation.

Supplementary data

Supplementary Figures S1 and S2 are available at *Mutagenesis* Online.

Funding

This work was supported by the Grant-in-Aid for Young Scientists (B) from the Ministry of Education, Culture, Sports, Science and Technology (B-22710068) and the Health, Welfare, and Labor Science Research Grants from the Japan Health Science Foundation (H24-food-general-011).

Acknowledgments

We are grateful to Drs F. Hanaoka (Gakushuin University, Tokyo) and C. Masutani (Nagoya University, Nagoya) for providing human pol η.

References

1. Lewis, J. G. and Adams, D. O. (1987) Inflammation, oxidative DNA damage, and carcinogenesis. *Environ. Health Perspect.*, **76**, 19–27.
2. Ames, B. N., Gold, L. S. and Willett, W. C. (1995) The causes and prevention of cancer. *Proc. Natl Acad. Sci. USA*, **92**, 5258–5265.
3. Ohshima, H. and Bartsch, H. (1994) Chronic infections and inflammatory processes as cancer risk factors: possible role of nitric oxide in carcinogenesis. *Mutat. Res.*, **305**, 253–264.
4. Weiss, S. J., Test, S. T., Eckmann, C. M., Roos, D. and Regiani, S. (1986) Brominating oxidants generated by human eosinophils. *Science*, **234**, 200–203.
5. Thomas, E. L., Bozeman, P. M., Jefferson, M. M. and King, C. C. (1995) Oxidation of bromide by the human leukocyte enzymes myeloperoxidase and eosinophil peroxidase. Formation of bromamines. *J. Biol. Chem.*, **270**, 2906–2913.
6. Klebanoff, S. J. (1968) Myeloperoxidase-halide-hydrogen peroxide antibacterial system. *J. Bacteriol.*, **95**, 2131–2138.
7. Harrison, J. E. and Schultz, J. (1976) Studies on the chlorinating activity of myeloperoxidase. *J. Biol. Chem.*, **251**, 1371–1374.
8. Foote, C. S., Goyne, T. E. and Lehrer, R. I. (1983) Assessment of chlorination by human neutrophils. *Nature*, **301**, 715–716.
9. Gaut, J. P., Yeh, G. C., Tran, H. D., *et al.* (2001) Neutrophils employ the myeloperoxidase system to generate antimicrobial brominating and chlorinating oxidants during sepsis. *Proc. Natl Acad. Sci. USA*, **98**, 11961–11966.
10. Babior, B. M. (2000) Phagocytes and oxidative stress. *Am. J. Med.*, **109**, 33–44.
11. Thukkani, A. K., Albert, C. J., Wildsmith, K. R., Messner, M. C., Martinson, B. D., Hsu, F. F. and Ford, D. A. (2003) Myeloperoxidase-derived reactive chlorinating species from human monocytes target plasmalogens in low density lipoprotein. *J. Biol. Chem.*, **278**, 36365–36372.
12. Domigan, N. M., Charlton, T. S., Duncan, M. W., Winterbourn, C. C. and Kettle, A. J. (1995) Chlorination of tyrosyl residues in peptides by myeloperoxidase and human neutrophils. *J. Biol. Chem.*, **270**, 16542–16548.
13. Hazen, S. L., Hsu, F. F., Mueller, D. M., Crowley, J. R. and Heinecke, J. W. (1996) Human neutrophils employ chlorine gas as an oxidant during phagocytosis. *J. Clin. Invest.*, **98**, 1283–1289.
14. Kang, J. I. Jr and Neidigh, J. W. (2008) Hypochlorous acid damages histone proteins forming 3-chlorotyrosine and 3,5-dichlorotyrosine. *Chem. Res. Toxicol.*, **21**, 1028–1038.
15. Masuda, M., Suzuki, T., Friesen, M. D., Ravanat, J. L., Cadet, J., Pignatelli, B., Nishino, H. and Ohshima, H. (2001) Chlorination of guanosine and other nucleosides by hypochlorous acid and myeloperoxidase of activated human neutrophils. Catalysis by nicotine and trimethylamine. *J. Biol. Chem.*, **276**, 40486–40496.
16. Henderson, J. P., Byun, J. and Heinecke, J. W. (1999) Molecular chlorine generated by the myeloperoxidase-hydrogen peroxide-chloride system of phagocytes produces 5-chlorocytosine in bacterial RNA. *J. Biol. Chem.*, **274**, 33440–33448.
17. Wiseman, H. and Halliwell, B. (1996) Damage to DNA by reactive oxygen and nitrogen species: role in inflammatory disease and progression to cancer. *Biochem. J.*, **313**, 17–29.
18. Henderson, J. P., Byun, J., Takeshita, J. and Heinecke, J. W. (2003) Phagocytes produce 5-chlorouracil and 5-bromouracil, two mutagenic products of myeloperoxidase, in human inflammatory tissue. *J. Biol. Chem.*, **278**, 23522–23528.
19. Jiang, Q., Blount, B. C. and Ames, B. N. (2003) 5-Chlorouracil, a marker of DNA damage from hypochlorous acid during inflammation. A gas chromatography-mass spectrometry assay. *J. Biol. Chem.*, **278**, 32834–32840.
20. Takeshita, J., Byun, J., Nhan, T. Q., Pritchard, D. K., Pennathur, S., Schwartz, S. M., Chait, A. and Heinecke, J. W. (2006) Myeloperoxidase generates 5-chlorouracil in human atherosclerotic tissue: a potential pathway for somatic mutagenesis by macrophages. *J. Biol. Chem.*, **281**, 3096–3104.
21. Kim, C. H., Darwanto, A., Theruvathu, J. A., Herring, J. L. and Sowers, L. C. (2010) Polymerase incorporation and miscoding properties of 5-chlorouracil. *Chem. Res. Toxicol.*, **23**, 740–748.
22. Morris, S. M. (1993) The genetic toxicology of 5-fluoropyrimidines and 5-chlorouracil. *Mutat. Res.*, **297**, 39–51.
23. Badouard, C., Masuda, M., Nishino, H., Cadet, J., Favier, A. and Ravanat, J. L. (2005) Detection of chlorinated DNA and RNA nucleosides by HPLC coupled to tandem mass spectrometry as potential biomarkers of inflammation. *J. Chromatogr. B Analyt. Technol Biomed. Life Sci.*, **827**, 26–31.
24. Whiteman, M., Jenner, A. and Halliwell, B. (1997) Hypochlorous acid-induced base modifications in isolated calf thymus DNA. *Chem. Res. Toxicol.*, **10**, 1240–1246.
25. Lao, V. V., Herring, J. L., Kim, C. H., Darwanto, A., Soto, U. and Sowers, L. C. (2009) Incorporation of 5-chlorocytosine into mammalian DNA results in heritable gene silencing and altered cytosine methylation patterns. *Carcinogenesis*, **30**, 886–893.
26. Valinluck, V. and Sowers, L. C. (2007) Inflammation-mediated cytosine damage: a mechanistic link between inflammation and the epigenetic alterations in human cancers. *Cancer Res.*, **67**, 5583–5586.
27. Asahi, T., Kondo, H., Masuda, M., *et al.* (2010) Chemical and immunochemical detection of 8-halogenated deoxyguanosines at early stage inflammation. *J. Biol. Chem.*, **285**, 9282–9291.
28. Hamm, M. L., Crowley, K. A., Ghio, M., *et al.* (2011) Importance of the C2, N7, and C8 positions to the mutagenic potential of 8-oxo-2′-deoxyguanosine with two A family polymerases. *Biochemistry*, **50**, 10713–10723.
29. Shibutani, S., Suzuki, N., Matsumoto, Y. and Grollman, A. P. (1996) Miscoding properties of 3,N4-etheno-2′-deoxycytidine in reactions catalyzed by mammalian DNA polymerases. *Biochemistry*, **35**, 14992–14998.
30. Yasui, M., Suenaga, E., Koyama, N., *et al.* (2008) Miscoding properties of 2′-deoxyinosine, a nitric oxide-derived DNA Adduct, during translesion synthesis catalyzed by human DNA polymerases. *J. Mol. Biol.*, **377**, 1015–1023.

31. Shibutani, S. (1993) Quantitation of base substitutions and deletions induced by chemical mutagens during DNA synthesis in vitro. *Chem. Res. Toxicol.*, **6**, 625–629.
32. Haracska, L., Prakash, L. and Prakash, S. (2002) Role of human DNA polymerase kappa as an extender in translesion synthesis. *Proc. Natl Acad. Sci. USA*, **99**, 16000–16005.
33. Zhang, Y., Yuan, F., Wu, X., Wang, M., Rechkoblit, O., Taylor, J. S., Geacintov, N. E. and Wang, Z. (2000) Error-free and error-prone lesion bypass by human DNA polymerase kappa in vitro. *Nucleic Acids Res.*, **28**, 4138–4146.
34. Haracska, L., Yu, S. L., Johnson, R. E., Prakash, L. and Prakash, S. (2000) Efficient and accurate replication in the presence of 7,8-dihydro-8-oxoguanine by DNA polymerase eta. *Nat. Genet.*, **25**, 458–461.
35. Zhang, Y., Wu, X., Guo, D., Rechkoblit, O. and Wang, Z. (2002) Activities of human DNA polymerase kappa in response to the major benzo[a]pyrene DNA adduct: error-free lesion bypass and extension synthesis from opposite the lesion. *DNA Repair*, **1**, 559–569.
36. Johnson, R. E., Prakash, S. and Prakash, L. (1999) Efficient bypass of a thymine-thymine dimer by yeast DNA polymerase, Poleta. *Science*, **283**, 1001–1004.
37. Masutani, C., Kusumoto, R., Yamada, A., *et al.* (1999) The XPV (xeroderma pigmentosum variant) gene encodes human DNA polymerase eta. *Nature*, **399**, 700–704.
38. Niimi, N., Sassa, A., Katafuchi, A., Grúz, P., Fujimoto, H., Bonala, R. R., Johnson, F., Ohta, T. and Nohmi, T. (2009) The steric gate amino acid tyrosine 112 is required for efficient mismatched-primer extension by human DNA polymerase kappa. *Biochemistry*, **48**, 4239–4246.
39. Fujikawa, K., Yakushiji, H., Nakabeppu, Y., Suzuki, T., Masuda, M., Ohshima, H. and Kasai, H. (2002) 8-Chloro-dGTP, a hypochlorous acid-modified nucleotide, is hydrolyzed by hMTH1, the human MutT homolog. *FEBS Lett.*, **512**, 149–151.
40. Yasui, M., Matsui, S., Ihara, M., Laxmi, Y. R., Shibutani, S. and Matsuda, T. (2001) Translesional synthesis on a DNA template containing N2-methyl-2′-deoxyguanosine catalyzed by the Klenow fragment of Escherichia coli DNA polymerase I. *Nucleic Acids Res.*, **29**, 1994–2001.
41. Mendelman, L. V., Petruska, J. and Goodman, M. F. (1990) Base mispair extension kinetics. Comparison of DNA polymerase alpha and reverse transcriptase. *J. Biol. Chem.*, **265**, 2338–2346.
42. Mendelman, L. V., Boosalis, M. S., Petruska, J. and Goodman, M. F. (1989) Nearest neighbor influences on DNA polymerase insertion fidelity. *J. Biol. Chem.*, **264**, 14415–14423.
43. Terashima, I., Suzuki, N., Dasaradhi, L., Tan, C. K., Downey, K. M. and Shibutani, S. (1998) Translesional synthesis on DNA templates containing an estrogen quinone-derived adduct: N2-(2-hydroxyestron-6-yl)-2′-deoxyguanosine and N6-(2-hydroxyestron-6-yl)-2′-deoxyadenosine. *Biochemistry*, **37**, 13807–13815.
44. Clark, J. M., Joyce, C. M. and Beardsley, G. P. (1987) Novel blunt-end addition reactions catalyzed by DNA polymerase I of *Escherichia coli*. *J. Mol. Biol.*, **198**, 123–127.
45. Johnson, R. E., Washington, M. T., Prakash, S. and Prakash, L. (2000) Fidelity of human DNA polymerase eta. *J. Biol. Chem.*, **275**, 7447–7450.
46. Sassa, A., Ohta, T., Nohmi, T., Honma, M. and Yasui, M. (2011) Mutational specificities of brominated DNA adducts catalyzed by human DNA polymerases. *J. Mol. Biol.*, **406**, 679–686.
47. Hamm, M. L., Rajguru, S., Downs, A. M. and Cholera, R. (2005) Base pair stability of 8-chloro- and 8-iodo-2′-deoxyguanosine opposite 2′-deoxycytidine: implications regarding the bioactivity of 8-oxo-2′-deoxyguanosine. *J. Am. Chem. Soc.*, **127**, 12220–12221.
48. Pyykkö, P. and Atsumi, M. (2009) Molecular single-bond covalent radii for elements 1-118. *Chemistry*, **15**, 186–197.
49. Sassa, A., Niimi, N., Fujimoto, H., *et al.* (2011) Phenylalanine 171 is a molecular brake for translesion synthesis across benzo[a]pyrene-guanine adducts by human DNA polymerase kappa. *Mutat. Res.*, **718**, 10–17.
50. Xu, P., Oum, L., Geacintov, N. E. and Broyde, S. (2008) Nucleotide selectivity opposite a benzo[a]pyrene-derived N2-dG adduct in a Y-family DNA polymerase: a 5′-slippage mechanism. *Biochemistry*, **47**, 2701–2709.
51. Shibutani, S., Suzuki, N. and Grollman, A. P. (2004) Mechanism of frameshift (deletion) generated by acetylaminofluorene-derived DNA adducts in vitro. *Biochemistry*, **43**, 15929–15935.
52. Garcia, A., Lambert, I. B. and Fuchs, R. P. (1993) DNA adduct-induced stabilization of slipped frameshift intermediates within repetitive sequences: implications for mutagenesis. *Proc. Natl. Acad Sci. USA*, **90**, 5989–5993.

DNA Repair 11 (2012) 259–266

Contents lists available at SciVerse ScienceDirect

DNA Repair

journal homepage: www.elsevier.com/locate/dnarepair

Activation of AMP-activated protein kinase by MAPO1 and FLCN induces apoptosis triggered by alkylated base mismatch in DNA

Teik How Lim[a], Ryosuke Fujikane[b], Shiori Sano[b,c], Ryuji Sakagami[c], Yoshimichi Nakatsu[a], Teruhisa Tsuzuki[a], Mutsuo Sekiguchi[d], Masumi Hidaka[b,*]

[a] Department of Medical Biophysics and Radiation Biology, Faculty of Medical Sciences, Kyushu University, Fukuoka 812-8582, Japan
[b] Department of Physiological Science and Molecular Biology, Fukuoka Dental College, Fukuoka 814-0193, Japan
[c] Department of Odontology, Fukuoka Dental College, Fukuoka 814-0193, Japan
[d] Frontier Research Center, Fukuoka Dental College, Fukuoka 814-0193, Japan

ARTICLE INFO

Article history:
Received 31 August 2011
Received in revised form 9 November 2011
Accepted 28 November 2011
Available online 29 December 2011

Keywords:
AMPK
Apoptosis
Folliculin/BHD
MAPO1/FNIP2/FNIPL
O^6-methylguanine

ABSTRACT

O^6-Methylguanine produced in DNA by the action of simple alkylating agents, such as *N*-methyl-*N*-nitrosourea (MNU), causes base-mispairing during DNA replication, thus leading to mutations and cancer. To prevent such outcomes, the cells carrying O^6-methylguanine undergo apoptosis in a mismatch repair protein-dependent manner. We previously identified MAPO1 as one of the components required for the induction of apoptosis triggered by O^6-methylguanine. MAPO1, also known as FNIP2 and FNIPL, forms a complex with AMP-activated protein kinase (AMPK) and folliculin (FLCN), which is encoded by the *BHD* tumor suppressor gene. We describe here the involvement of the AMPK–MAPO1–FLCN complex in the signaling pathway of apoptosis induced by O^6-methylguanine. By the introduction of siRNAs specific for these genes, the transition of cells to a population with sub-G_1 DNA content following MNU treatment was significantly suppressed. After MNU exposure, phosphorylation of AMPKα occurred in an MLH1-dependent manner, and this activation of AMPK was not observed in cells in which the expression of either the *Mapo1* or the *Flcn* gene was downregulated. When cells were treated with AICA-ribose (AICAR), a specific activator of AMPK, activation of AMPK was also observed in a MAPO1- and FLCN-dependent manner, thus leading to cell death which was accompanied by the depolarization of the mitochondrial membrane, a hallmark of the apoptosis induction. It is therefore likely that MAPO1, in its association with FLCN, may regulate the activation of AMPK to control the induction of apoptosis triggered by O^6-methylguanine.

1. Introduction

Most of the DNA lesions produced by internal and external agents can be removed by cellular DNA repair enzymes, while cells with un-repaired lesions are eliminated by apoptosis. The biological significance of these two mechanisms is clearly shown when organisms lacking one or both of these cellular functions are exposed to simple alkylating agents, such as *N*-methyl-*N*-nitrosourea (MNU) and *N*-methyl-*N'*-nitro-*N*-nitrosoguanidine (MNNG), which alkylate purine and pyrimidine bases in DNA [1]. Among the various modified bases thus produced, O^6-methylguanine is of particular importance since this modified base can pair with thymine as well as cytosine during DNA replication, leading to induction of mutation and cancer [2,3]. Organisms possess a specific DNA repair enzyme, O^6-methylguanine-DNA methyltransferase (MGMT), which transfers a methyl-group from O^6-methylguanine in DNA onto the enzyme molecule, thereby repairing the DNA lesion in a single step reaction [4,5]. When the modified base is not repaired, an O^6-methylguanine–thymine pair is formed through DNA replication and this mismatch can be recognized by a mismatch repair protein complex, composed of MSH2, MSH6, MLH1 and PMS2, which induces apoptosis to exclude cells carrying the mutation-evoking DNA lesions [6–8]. It is noteworthy that $Mgmt^{-/-}$ mice, which lack the DNA repair enzyme specific for O^6-methylguanine, are hypersensitive to both the killing and to the tumorigenic action of alkylating chemicals [9–12] and these dual effects can be dissociated by the introduction of an additional defect in mismatch repair genes. Mice with mutations in both alleles of the *Mgmt* and the *Mlh1* genes, the latter encoding a protein involved in the recognition of mismatched base, are as resistant to MNU as are wild-type mice in terms of survival, but are much more susceptible to MNU-induced tumorigenesis than wild-type mice

* Corresponding author at: Department of Physiological Science and Molecular Biology, Fukuoka Dental College, 2-15-1 Tamura, Sawara-ku, Fukuoka 814-0193, Japan. Tel.: +81 92 801 0411x310; fax: +81 92 801 0685.
E-mail address: hidaka@college.fdcnet.ac.jp (M. Hidaka).

1568-7864/$ – see front matter © 2011 Elsevier B.V. All rights reserved.
doi:10.1016/j.dnarep.2011.11.006

[13]. Consistent with these results, *Mgmt*$^{-/-}$ *Mlh1*$^{-/-}$ cells, derived from the gene-targeted mice, are unable to induce apoptosis and show an elevated mutant frequency after MNU treatment [14].

The apoptotic signal initiated through the mismatch recognition complex activates a signaling cascade leading to the cell cycle checkpoints and apoptotic pathways for cell death. Both the release of cytochrome C from the mitochondria as well as the activation of Apaf-1 and caspase-3, hallmarks of the induction of apoptosis, have been demonstrated after the treatment of cells with alkylating agents that produce O^6-methylguanine [14,15]. However, the precise molecular mechanism underlying the signal transduction downstream of mismatch recognition still remains to be determined. To identify the factors involved in the O^6-methylguanine-induced apoptotic process, we screened MNU-resistant clones derived from MNU-sensitive *Mgmt*$^{-/-}$ cells using retrovirus-mediated gene-trap mutagenesis [16]. Mouse-derived KH101 cells, carrying an insertional mutation in one of the alleles of an uncharacterized gene, were unable to induce mitochondrial membrane depolarization as well as caspase-3 activation, after treatment with MNU. In this way, we identified a new gene, designated as *Mapo1* (O^6-methylguanine induced apoptosis 1), which was related to the induction of apoptosis. The mutant frequency of KH101 cells was significantly elevated after the treatment with MNU, thus supporting the notion that the induction of apoptosis, in which the MAPO1 is involved, contributes significantly to the elimination of cells carrying mutation-inducing DNA lesions. A search in the database revealed that the amino acid sequence of the MAPO1 protein is homologous to that of folliculin-interacting protein 1 (FNIP1), which was identified as a protein having the capacity to associate with folliculin [17]. Folliculin is a tumor suppressor protein with unknown biological activity, and is encoded by the *FLCN* gene. Mutations in the *FLCN* gene have been found in patients with Birt-Hogg-Dubé (BHD) syndrome [18,19], which is characterized by the development of hair follicle hamartomas, lung cysts, and an increased risk for renal neoplasia [20–22]. Identification of another folliculin-interacting protein, displaying a similarity in its amino acid sequence to that of FNIP1, was reported by two groups of researchers and the gene responsible was named *FNIP2* and *FNIPL*, respectively [23,24]. The *FNIP2/FNIPL* gene turned out to be the same gene as the human homolog of *Mapo1*. It was also reported that FNIP2/FNIPL, as well as FNIP1, could bind to 5′-AMP-activated protein kinase (AMPK), composed of AMPKα, β and γ subunits, which is an important energy sensor in cells that negatively regulates cell growth and proliferation [25,26].

We report here that a complex composed of MAPO1, FLCN and AMPK is involved in the induction of apoptosis triggered by O^6-methylguanine–thymine mispair. Evidence is presented which shows that during the course of apoptosis induction, the phosphorylation of AMPKα occurs in a MAPO1- and FLCN-dependent manner.

2. Materials and methods

2.1. Cell lines and cell culture

The YT102 (*Mgmt*$^{-/-}$ *Mlh1*$^{+/+}$), YT103 (*Mgmt*$^{-/-}$ *Mlh1*$^{-/-}$) and KH101 (*Mgmt*$^{-/-}$ *Mapo1*$^{+/-}$) cell lines were established as described previously [14,16]. The cells were cultivated in Dulbecco's modified Eagle's medium (D-MEM) supplemented with 10% fetal bovine serum (FBS) at 37 °C in 5% CO_2.

2.2. Chemicals

N-Methyl-*N*-nitrosourea (MNU) was obtained from Sigma. Compound C and AICA-Ribose were purchased from Calbiochem.

2.3. Immunoprecipitation and immunoblotting

To prepare cells expressing Flag-tagged MAPO1 or HA-tagged FLCN, a pIRES-puro3 vector (Clontech) containing mouse-derived *Mapo1* cDNA tagged with Flag epitope at the carboxy terminal end or a pIRES-puro2 (Clontech) vector carrying mouse-derived *Flcn* cDNA tagged with the HA epitope at the amino terminal end was introduced into YT102 cells using Lipofectamine 2000 (Invitrogen) according to the manufacturer's protocol. For the immunoprecipitation, the cells were lysed with NETN buffer (50 mM Tris/HCl (pH 8.0), 150 mM NaCl, 0.2% NP-40, 1 mM EDTA) containing protease inhibitors (Roche). To precipitate the Flag-tagged MAPO1, 10 μl of anti-FLAG M2-agarose (Sigma) were added to the extract, and incubated for 4 h at 4 °C. Alternatively, 10 μl of anti-HA (HA-7)-agarose (Sigma) were added to precipitate the HA-tagged FLCN, and the mixture was incubated overnight at 4 °C. After extensive washing of the beads with NETN buffer, the proteins bound to the beads were eluted in 40 μl of 2× SDS-PAGE sample buffer (120 mM Tris/HCl (pH 6.8), 4% SDS, 20% glycerol, 200 mM DTT, 0.002% bromophenol blue).

For the immunoblotting analyses, immunoprecipitated materials or whole cell extracts prepared by the lysis of cells with 2× SDS-PAGE sample buffer were subjected to SDS-PAGE and electroblotted onto a PVDF membrane (Bio-Rad). Detection was performed using an ECL Plus or Advance Western blotting detection kit (GE Healthcare). The primary antibodies used were: anti-FLAG M2 (Sigma), anti-HA HA-7 (Sigma), anti-FLCN (Protein Tech Group, Inc.), anti-AMPKα (Cell signaling), anti-β-actin (Sigma), and anti-phospho-AMPKα (Thr172) (Cell signaling). Anti-mouse IgG and anti-rabbit IgG conjugated to horseradish peroxidase (GE Healthcare) were used as the secondary antibodies.

2.4. siRNA transfection

Stealth RNAi for the *Mapo1* gene (siMapo1), 5′-CAGAAAGCAGAGGAUGUUCCUAUUA-3′, *Flcn* gene (siFlcn#1), 5′-UUAUUCAGGAUAGUGGGCCCAACUC-3′, (siFlcn#2), 5′-UGGUGACUGACGUACUUAAUAGAGG-3′, and *Ampkα* gene (siAmpkα#1), 5′-UAUCUUAGCGUUCAUCUGGGCAUCC-3′, (siAmpkα#2), 5′-AAGAUGAUAAGCCACUGCAAGCUGG-3′ were purchased from Invitrogen. After culturing 1×10^5 cells in a 6-well plate for one day, the cells were transfected with 20 nM siRNA, using the Lipofectamine RNAiMAX reagent (Invitrogen) according to the manufacturer's protocol. For the control transfection, Stealth RNAi Negative Control Medium GC Duplex (Invitrogen) was used.

2.5. Flow cytometric analysis

For the sub-G_1 population assay, cells were washed with PBS and suspended in 400 μl of PBS containing 0.1% Triton X-100, 25 μg/ml of propidium iodide and 0.1 mg/ml of RNase A. The samples were analyzed using a FACS Calibur flow cytometer (Becton Dickinson), with 10,000 events per determination.

For the mitochondrial membrane depolarization assay, cells were treated with the MitoProbeTM DiOC2(3) Assay Kit (Invitrogen), according to the manufacturer's protocol, and then subjected to analysis using a FACS Calibur flow cytometer.

2.6. Trypan blue exclusion assay

The viability of YT102, KH101 and siRNA-transfected YT102 cells was assayed, based on their trypan blue exclusion. The cells treated with AICA-Ribose were collected 48 h after the drug treatment and were stained with 0.2% trypan blue. The percentage of dead cells was determined as the percentage of trypan blue staining-positive cells. At least 500 cells were counted per experiment.

2.7. Statistics

All *P*-values were generated using two-tailed Student's *t*-tests.

3. Results

3.1. Interaction of MAPO1 with FLCN and AMPK

To confirm that MAPO1 protein interacts with FLCN and AMPK, a co-immunoprecipitation experiment was performed. Whole cell extracts were prepared from mouse YT102 (*Mgmt*$^{-/-}$) cells expressing Flag-tagged MAPO1, and were subjected to immunoprecipitation using an anti-Flag antibody conjugated to agarose beads. The results are shown in Fig. 1A. With whole cell extracts, almost the same intensity of bands for FLCN and AMPKα were detected in both control and Flag-MAPO1-transfected cells. When the materials were immunoprecipitated with the anti-Flag antibody, co-precipitated FLCN and AMPKα were clearly detected, concomitant with the effective precipitation of Flag-MAPO1, whereas no such bands were seen in a sample precipitated from cells treated with the control vector alone.

To evaluate the interaction of FLCN with MAPO1 and AMPK in a reciprocal manner, whole cell extracts prepared from YT102 cells expressing FLAG-tagged MAPO1, with or without HA-tagged FLCN, were applied for immunoprecipitation using an anti-HA antibody (Fig. 1B). When the HA-tagged FLCN was precipitated, as indicated by doublet bands by the immunoblotting analysis, the Flag-tagged MAPO1 and AMPKα were co-precipitated. It is evident, therefore, that MAPO1 interacts with FLCN and AMPK in mouse cells.

3.2. Suppression of the induction of apoptosis in Flcn- and Ampkα-knockdown cells

Since MAPO1 has been identified as an apoptosis-inducing protein, it is plausible that the MAPO1-bound proteins, FLCN and AMPK, might also be involved in apoptosis induction. To examine the possible roles of these proteins, siRNAs specific for the *Flcn* or *Ampkα* genes were introduced into YT102 (*Mgmt*$^{-/-}$) cells. As shown in Fig. 2A and B, two independent siRNAs (siFlcn#1 and #2, and siAmpkα#1 and #2), designed at different sequences of each gene, effectively suppressed the expression of the genes when measured at 48 h after their introduction. The expression level of the *Mapo1* gene in siMapo1-treated cells also decreased to 43% of that in cells that were treated with the control RNA, siCont, as measured by quantitative real time PCR [16]. To monitor the appearance of cells with sub-G_1 DNA content, cells were treated with or without 0.4 mM MNU for 1 h and subjected to a flow cytometric analysis 72 h later. After treatment with MNU, the sub-G_1 cell population increased to more than 20% in the siCont-treated cells (Fig. 2C). Under the same conditions, the degrees of the increases in the cells treated with siRNAs against the *Flcn*, *Ampkα* and *Mapo1* genes were significantly suppressed. These results favor the notion that FLCN and AMPKα, as well as MAPO1, are involved in MNU-induced apoptosis through protein interactions.

3.3. Suppression of the induction of apoptosis by an AMPK inhibitor

The effects of *Ampkα* knockdown on the MNU-induced apoptosis were further examined at multiple time points. The YT102 cells transfected with siCont or siAmpkα#2 were exposed to 0.4 mM MNU for 1 h and then subjected to a flow cytmetric analysis. As shown in Fig. 3A, the sub-G_1 cell population increased gradually, with similar kinetics in cells transfected with either type of siRNA, but the degree of the increase in cells transfected with siAmpkα was significantly lower than that of siCont-transfected cells.

To obtain further evidence supporting the involvement of AMPK in MNU-induced apoptosis, compound C, a specific inhibitor of AMPK, was used to downregulate the function of AMPK. YT102 cells were exposed to 0.4 mM MNU for 1 h, followed by incubation with or without 2 μM of compound C for 72 h, and then cells were subjected to a flow cytometric analysis. As shown in Fig. 3B, the sub-G_1 cell population in compound C-treated cells after MNU treatment significantly decreased in comparison to those not treated with the inhibitor. The inhibitory effects of compound C on AMPK activity were assessed by immunoblotting using an antibody that specifically recognizes a phosphorylated form of AMPKα, since AMPK is activated when the catalytic subunit of AMPKα becomes phosphorylated [27–29]. As shown in Fig. 3C, AMPK appeared to be activated after MNU treatment, while such activation was significantly suppressed by the exposure of cells to compound C. These findings are consistent with the notion that AMPK plays an important role in the induction of apoptosis triggered by MNU.

3.4. MAPO1- and FLCN-dependent activation of AMPK during the induction of apoptosis

To further examine if AMPKα is phosphorylated during the induction of apoptosis, YT102 cells were treated with 1 mM MNU and then collected at 0, 24, 48 and 72 h after treatment. Under these conditions, apoptosis was effectively induced, as was evident by the detection of the mitochondrial membrane depolarization and the caspase-3 activity [16]. The whole cell extracts were prepared, and the phosphorylation levels of AMPKα were assessed by

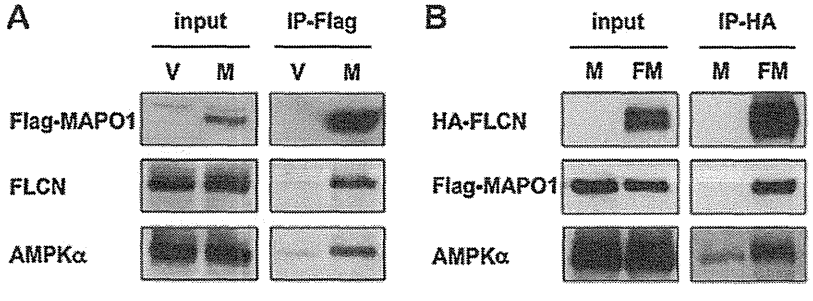

Fig. 1. The association of MAPO1, FLCN and AMPKα proteins. (A) The interaction of MAPO1 with FLCN and AMPKα. YT102 cells were transfected with the pIRES-puro3 vector (termed as V) or pIRES-puro3 containing Flag-tagged *Mapo1* cDNA (termed as M) and harvested after incubation for 24 h. Whole cell extracts (input) were used for immunoprecipitation using anti-Flag M2 antibody beads (IP-Flag). The materials were subjected to SDS-PAGE, transferred to a membrane and immunoblotted using antibodies that recognize the Flag-tag, FLCN and AMPKα. (B) The interaction of FLCN with MAPO1 and AMPKα. YT102 cells were transfected with either pIRES-puro3 containing Flag-tagged *Mapo1* cDNA (termed as M) or pIRE-puro2 carrying HA-tagged *Flcn* cDNA and pIRES-puro3 containing Flag-tagged *Mapo1* cDNA (termed as FM) and were harvested 24 h later. Following immunoprecipitation using anti-HA HA7 antibody beads (IP-HA), an immunoblotting analysis was performed as described in (A) with anti-HA, anti-Flag and anti-AMPKα antibodies.

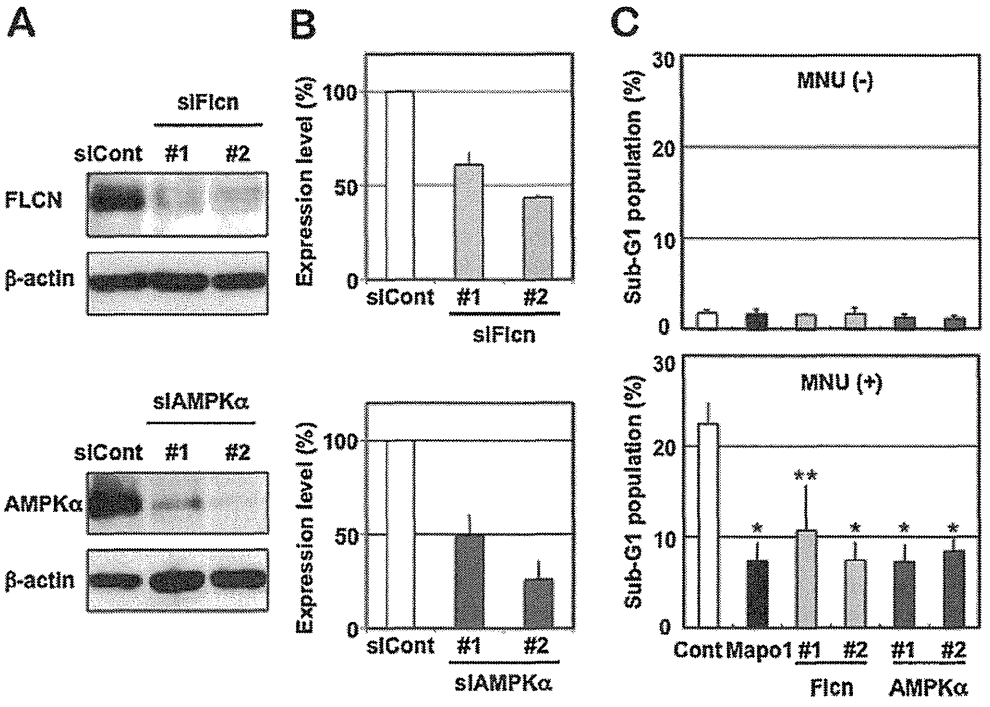

Fig. 2. The suppression of apoptosis by siRNAs targeting the three types of genes. (A) The expression levels of FLCN and AMPKα in cells treated with siRNAs. The whole extracts of YT102 cells transfected with control and two independent siRNAs specific for the corresponding genes were used for the immunoblotting analysis with antibodies specific for FLCN, AMPKα and β-actin (loading control). (B) The relative expression levels of FLCN and AMPKα in the cells treated with siRNAs, as measured by an immunoblotting analysis in (A). (C) The sub-G_1 population of cells transfected with control, *Mapo1*-, *Flcn*- or *Ampkα*-siRNA after MNU treatment. Two days after transfection with siRNA, YT102 cells were treated with or without 0.4 mM MNU for 1 h and then incubated for three days. The cells were harvested and subjected to a flow cytometric analysis. $^{*}P<0.01$; $^{**}P<0.05$ when comparing the sub-G_1 populations in the control and gene-specific siRNA-transfected cells.

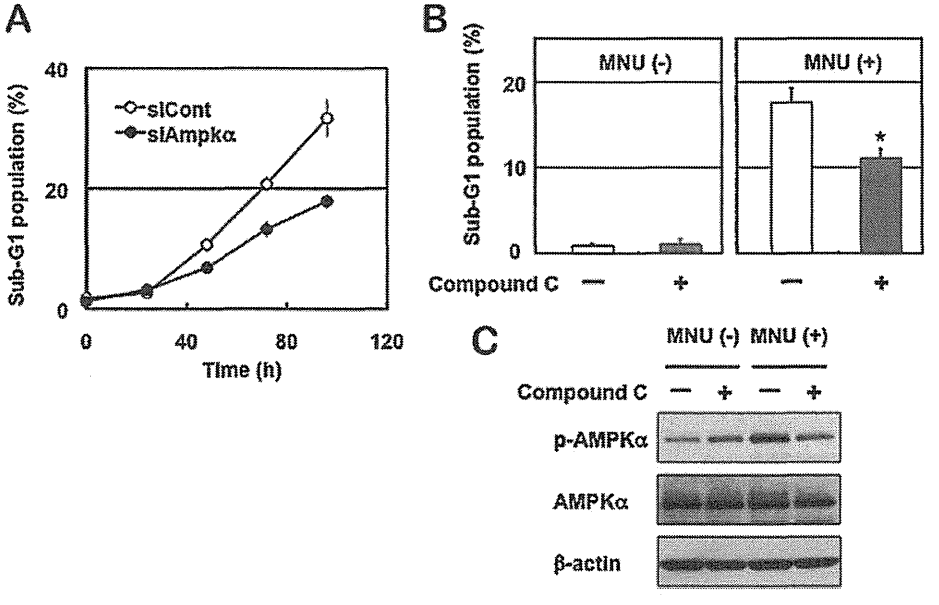

Fig. 3. The involvement of AMPK in MNU-induced apoptosis. (A) The sub-G_1 population of cells transfected with control or *Ampkα* siRNA after MNU treatment. Two days after transfection with siRNA, the YT102 cells were treated with 0.4 mM MNU for 1 h and then harvested at 0, 24, 48, 72 and 96 h after MNU treatment, and subjected to a flow cytometric analysis. The numbers of the cells in the sub-G_1 population were counted and the ratios were plotted. Open circles, siCont-transfected cells; closed circles, siAmpkα-transfected cells. (B) The suppression of apoptosis by an AMPK inhibitor. After treatment with or without 0.4 mM MNU for 1 h, YT102 cells were incubated in medium supplemented with or without 2 μM compound C for three days. The cells were then harvested and subjected to a flow cytometric analysis to monitor the sub-G_1 population of cells. $^{*}P<0.01$ when comparing the sub-G_1 populations in compound C-untreated and compound C-treated cells after exposure to MNU. (C) The inhibition of the AMPK activity by compound C. The whole cell extracts from the cells harvested at 48 h after MNU treatment were subjected to an immunoblotting analysis using antibodies that recognize phospho-AMPKα (Thr172), AMPKα and β-actin, respectively.

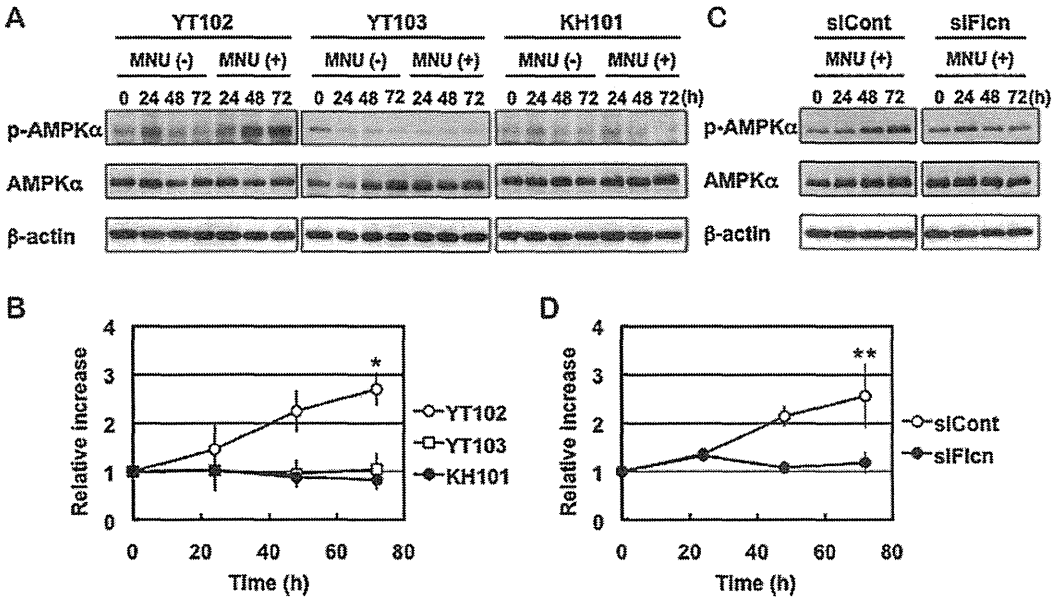

Fig. 4. The activation of AMPK after MNU treatment. (A) The phosphorylation of AMPKα in cells with different genetic backgrounds. Three cell lines, YT102 (*Mgmt*$^{-/-}$), YT103 (*Mgmt*$^{-/-}$ *Mlh1*$^{-/-}$) and KH101 (*Mgmt*$^{-/-}$ *Mapo1*$^{+/-}$), were treated with or without 1 mM MNU for 1 h and then incubated for 0, 24, 48 or 72 h. The whole cell extracts from cells harvested at various times after MNU treatment were subjected to an immunoblotting analysis using antibodies that recognize phospho-AMPKα (Thr172), AMPKα and β-actin, respectively. (B) The relative intensities of the bands for phospho-AMPKα (Thr172) after MNU treatment. Open circles, YT102; open squares, YT103; closed circles, KH101. *$P < 0.01$ when comparing the relative intensities for YT102 cells with those of the YT103 and KH101 cells at 72 h after exposure to MNU. (C) Activation of AMPK in cells transfected with *Flcn*-siRNA. Two days after transfection with control or *Flcn*-siRNA, the YT102 cells were treated with or without 1 mM MNU for 1 h. The analysis was performed as described above. (D) The relative intensities of bands for phospho-AMPKα (Thr172) after MNU treatment. Open circles, siCont-transfected cells; closed circles, siFlcn-transfected cells. **$P < 0.05$ when comparing the relative intensities of the control and *Flcn*-specific siRNA-transfected cells at 72 h after exposure to MNU.

an immunoblotting analysis. As shown in Fig. 4A and B, the levels of phosphorylation of AMPKα increased gradually and reached about 2.7-folds at 72 h after MNU treatment, whereas no such increase was observed in cells not expose to MNU. The amounts of the AMPKα protein were almost constant under these situations. In YT103 (*Mgmt*$^{-/-}$ *Mlh1*$^{-/-}$) cells, which are unable to induce apoptosis due to their lack of the *Mlh1* gene, the increase of phosphorylated forms of AMPKα was hardly detectable, even after MNU treatment. These results indicate that AMPK is activated during the course of the induction of apoptosis, triggered in a mismatch repair protein-dependent manner. To evaluate the effects of *Mapo1* mutation on the activation of AMPK, we used KH101 (*Mgmt*$^{-/-}$ *Mapo1*$^{+/-}$) cells, which carry an insertional mutation in one of the alleles of the *Mapo1* gene and exhibit haploinsufficiency for the induction of apoptosis triggered by MNU treatment [16]. Similar to the results described above, no increase in the band corresponding to phosphorylated AMPKα was detected even after treatment with MNU (Fig. 4A and B). Since MAPO1 interacts with FLCN (Fig. 1), it was supposed that FLCN might also play a role in the activation of AMPK during the course of apoptosis. To examine this possibility, YT102 (*Mgmt*$^{-/-}$) cells were transfected with siRNA targeting the *Flcn* gene (siFlcn#2), and then were exposed to 1 mM MNU for 1 h. The immunoblotting analyses of these samples collected after incubation for 0, 24, 48 and 72 h revealed that phosphorylation of AMPKα, which occurred gradually in siCont-transfected cells, did not take place in the siFlcn-transfected ones (Fig. 4C and D). These results indicate that the activation of AMPK, which occurs during the course of MNU-induced apoptosis, is dependent on the functions of both FLCN and MAPO1.

3.5. Induction of apoptosis through activation of AMPK

To confirm the importance of the activation of AMPK for the induction of apoptosis, AICA-Ribose (AICAR), a specific activator of AMPK, was applied to YT102 cells. After treatment with a low dose (0.2 mM) of AICAR for 48 h, the viabilities of cells were analyzed, based on the trypan blue exclusion assay. As shown in Fig. 5A, there was a significant increase of trypan blue staining-positive cells after treatment with AICAR in the YT102 (*Mgmt*$^{-/-}$ *Mapo1*$^{+/+}$) cells, whereas no such increase was observed in the *Mapo1*-defective KH101 (*Mgmt*$^{-/-}$ *Mapo1*$^{+/-}$) cells even after the same treatment. To determine if the increase in dead cells was related to the induction of apoptosis, the cells were subjected to an assay for mitochondrial membrane depolarization, which is known to occur during the process of apoptosis. The results are shown in Fig. 5B and C. The depolarization of the mitochondrial membrane was induced after treatment with AICAR in YT102 cells, but not in *Mapo1*-defective KH101 cells. The results indicate that the function of MAPO1 is necessary for AICAR-induced apoptosis. An immunoblotting experiment, the results of which are shown in Fig. 5D, revealed that the AICAR-treatment induced phosphorylation of AMPKα to the similar level to that when treated with MNU, however, such an induction did not occur in the *Mapo1*-defective KH101 cells. These results suggest that the activation of AMPK is important for the induction of apoptosis, and that a normal level of MAPO1 is necessary for the activation of AMPK.

We next examined if FLCN, which interacts with MAPO1, is also required for the AICAR-induced cell death. For this study, we applied AICAR to YT102 cells whose FLCN function was knocked down by siRNA (siFlcn#2). As shown in Fig. 6A–C, the degree of AICAR-induced cell death, which was accompanied by the depolarization of the mitochondrial membrane, was significantly lower in siFlcn-transfected cells as compared to that in siCont-transfected ones. Furthermore, the AICAR-induced AMPKα phosphorylation was almost completely blocked in siFlcn-transfected cells (Fig. 6D). Therefore, these results suggest that FLCN is required for AMPK activation, as well as the cell death induced by the treatment with AICAR.

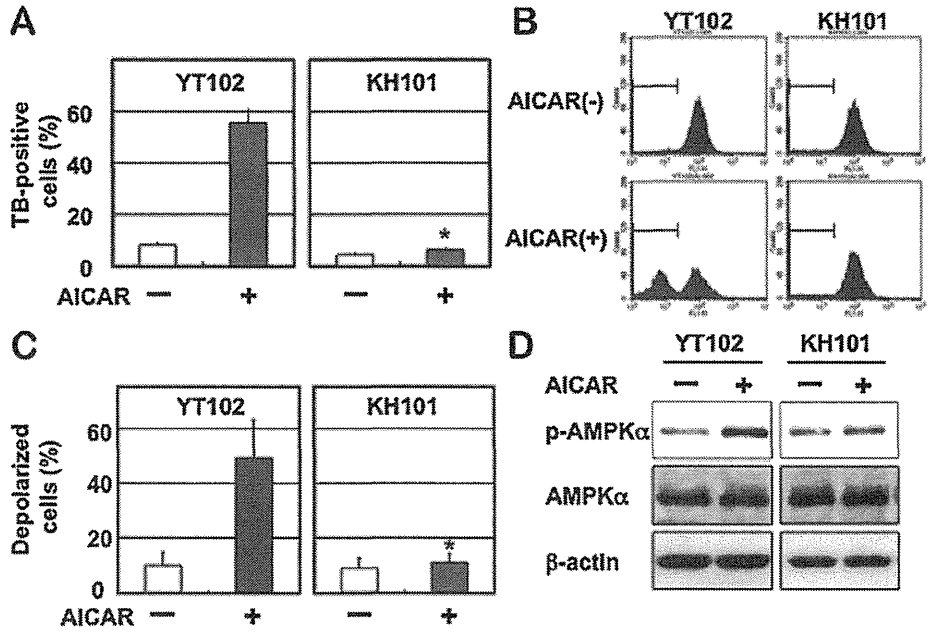

Fig. 5. MAPO1-dependent cell death induced by an AMPK activator. *Mapo1*-proficient YT102 and *Mapo1*-defective KH101 cells were incubated in a medium supplemented with or without 0.2 mM AICAR for two days and then harvested. (A) The viabilities of the cells. The numbers of cells stained with trypan blue (TB) were counted and the ratios are shown. $^{*}P < 0.01$ when comparing the TB-positive YT102 and KH101 cells after exposure to AICAR. (B) Depolarization of the mitochondrial membrane. The cells were evaluated by a mitochondrial membrane depolarization assay, and representative patterns of the assay are shown. The populations of depolarized cells were gated by bars. (C) The levels of mitochondrial membrane depolarization. The mean values obtained from three independent experiments in (B) and the standard deviations (bars) are presented. $^{*}P < 0.01$ when comparing the depolarized cells in YT102 and KH101 cells after exposure to AICAR. (D) Activation of AMPK after treatment with AICAR. The whole cell extracts prepared from cells, treated with or without AICAR, were subjected to an immunoblotting analysis using antibodies specific for phospho-AMPKα (Thr172), AMPKα and β-actin, respectively.

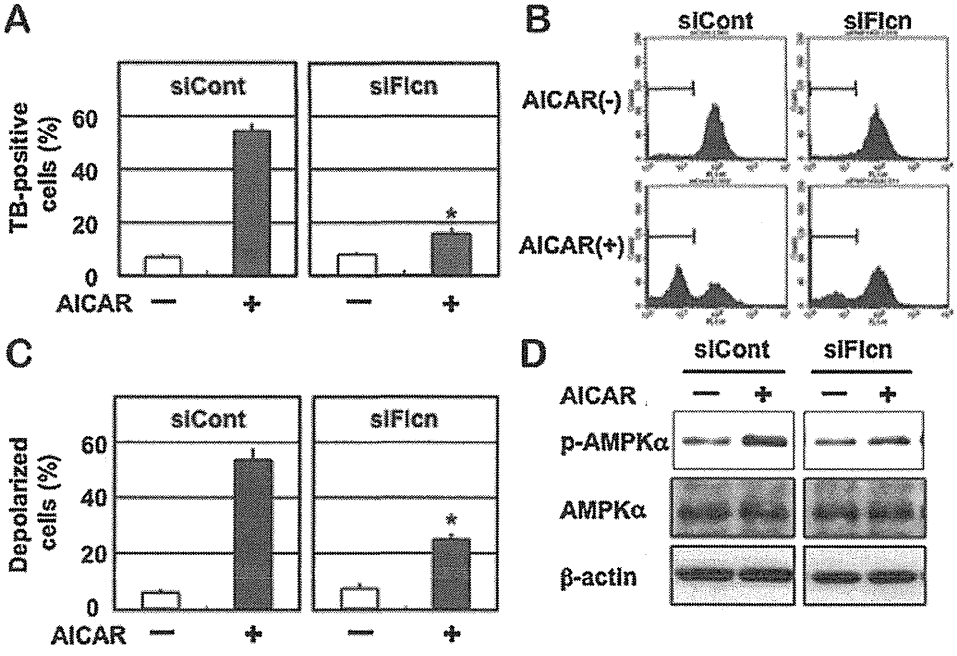

Fig. 6. FLCN-dependent cell death induced by an AMPK activator. YT102 cells transfected with control- or *Flcn*-siRNA were cultured with or without 0.2 mM AICAR for two days and then harvested. (A) The viabilities of the cells. The numbers of cells stained with trypan blue (TB) were counted and the ratios are shown. $^{*}P < 0.01$ when comparing the TB-positive siCont-transfected and siFlcn-transfected cells after exposure to AICAR. (B) Depolarization of the mitochondrial membrane. The cells were evaluated by a mitochondrial membrane depolarization assay, and representative patterns of the assay are shown. The populations of depolarized cells were gated by bars. (C) The levels of mitochondrial membrane depolarization. The mean values obtained from three independent experiments in (B) and the standard deviations (bars) are presented. $^{*}P < 0.01$ when comparing the depolarized cells in siCont-transfected and siFlcn-transfected cells after exposure to AICAR. (D) Activation of AMPK after treatment with AICAR. The whole cell extracts prepared from AICAR-treated or -untreated cells, were subjected to an immunoblotting analysis using antibodies specific for phospho-AMPKα (Thr172), AMPKα and β-actin, respectively.

4. Discussion

MAPO1 was identified as one of the protein elements functioning at a certain step following the induction of apoptosis [16]. In *Mapo1*-defective cells, mitochondrial membrane depolarization and caspase-3 activation were not observed even after exposure to MNU, although the cells retain the ability for mismatch repair protein-dependent DNA damage detection and signaling. Subsequent studies have revealed that MAPO1 is identical to FNIP2 and FNIPL, reported by Hasumi et al. [23] and Takagi et al. [24], respectively. This protein is bound to folliculin, encoded by the *FLCN* tumor suppressor gene, and AMP-activated protein kinase (AMPK). To analyze the possible roles of folliculin and AMPK in the induction of apoptosis, we introduced siRNAs specific for the *Flcn* or *Ampkα* gene and then treated the cells with MNU. The flow cytometric analyses performed to measure the sub-G_1 population of cells revealed that folliculin and AMPK, as well as MAPO1, were involved in MNU-induced apoptosis. Taken together, these data suggest that MAPO1 forms a protein complex(es) with folliculin and AMPK, and plays a role in a signal transduction pathway of apoptosis.

It is known that AMPK is one of the signaling kinases that negatively regulates cell growth and proliferation and is phosphorylated itself under conditions of energetic stress [26–29]. Several recent papers have observed the pro-apoptotic potential of activated AMPK [30–33]. In this report, we found a gradual increase in the levels of AMPK phosphorylation in *Mapo1*-proficient cells after MNU treatment, implying a possible involvement of the activation of AMPK in the MNU-induced apoptosis pathway. In *Mapo1*-deficient cells, AMPK activation in this manner was hardly detectable, even after the treatment with MNU. Furthermore, the treatment of cells with AICAR, a specific activator of AMPK, resulted in AMPKα phosphorylation and mitochondrial membrane depolarization in a *Mapo1*-dependent manner. These findings extended onto the case of *Flcn*-knockdown cells. Taken together, it is likely that MAPO1 and FLCN positively regulate the activation of AMPK through their mutual interaction in the apoptotic signaling pathway, triggered by an alkylating agent. MAPO1 and FLCN proteins have been reported to undergo some modifications in cells [17,24]. The treatment with an alkylating agent might affect the modified states of these proteins, and might cause the activation of the protein complex, thus leading to AMPK activation. Another folliculin-interacting protein, FNIP1, which is homologous to MAPO1, is also capable of binding to AMPK [17]. The activation of AMPK might therefore be regulated in more complex ways under the balance of MAPO1 and FNIP1 activities.

Another important problem which remains to be solved is how the AMPK–MAPO1–FLCN complex is activated by the signal delivered from the mismatch repair protein complex, which itself is activated through the interaction with DNA carrying base mismatches. The signal may be delivered by direct physical contact between the two complexes or through the involvement of other protein factors. The protein linking analyses, aided by mass spectrometry, have been performed, but no evidence to show the physical association of the two complexes was obtained (unpublished results). It seems likely, therefore, that some other protein factor(s) might be involved in the signal transduction process. To identify such factors, it would be relevant to extend this approach using retrovirus-mediated gene-trap mutagenesis studies.

Germline mutations in the *FLCN* gene have been identified in patients with Birt-Hogg-Dubé (BHD) syndrome, which is an autosomal dominant disorder characterized by hamartomas of skin follicles, spontaneous pneumothorax, and renal tumors [20–22]. Furthermore, *BHD* heterozygous knockout mice were revealed to develop kidney cysts and tumors as they aged, while *BHD* homozygous null mice displayed early embryonic lethality [34,35]. The recent findings, including this report, strongly suggest that folliculin has physical and/or functional interactions with the AMPK-mTOR signaling pathway [17,34,36]. Mutations in several other tumor suppressor genes, such as *LKB1*, *TSC1* and *TSC2* [29,37], have also been shown to lead to dysregulation of AMPK-mTOR signaling and to the development of other hamartomatous syndromes. Our present findings that folliculin is involved in the induction of apoptosis might shed some light on the physiological roles of *BHD/FLCN* and other related tumor suppressor genes. We are currently establishing *Mapo1* knockout mice to analyze the possible roles of the gene in the suppression of tumor predisposition resulting from environmental stresses.

Conflict of interest statement

The authors declare that there are no conflicts of interests.

Acknowledgments

We thank Drs. H. Hayakawa and Y. Takagi (Fukuoka Dental College, Japan) for helpful discussion. This work was supported by grants (including a Frontier Research Grant) from the Ministry of Education, Culture, Sports, Science and Technology of Japan, and from the Ministry of Health, Labor and Welfare of Japan.

References

[1] D.T. Beranek, Distribution of methyl and ethyl adducts following alkylation with monofunctional alkylating agents, Mutat. Res. 231 (1990) 11–30.
[2] C. Coulondre, J.H. Miller, Genetic studies of the lac repressor. IV. Mutagenic specificity in the lacI gene of *Escherichia coli*, J. Mol. Biol. 117 (1977) 577–606.
[3] T. Ito, T. Nakamura, H. Maki, M. Sekiguchi, Roles of transcription and repair in alkylation mutagenesis, Mutat. Res. 314 (1994) 273–285.
[4] B. Demple, A. Jacobsson, M. Olsson, P. Robins, T. Lindahl, Repair of alkylated DNA in *Escherichia coli*. Physical properties of O6-methylguanine–DNA methyltransferase, J. Biol. Chem. 257 (1982) 13776–13780.
[5] H. Kawate, K. Ihara, K. Kohda, K. Sakumi, M. Sekiguchi, Mouse methyltransferase for repair of O6-methylguanine and O4-methylthymine in DNA, Carcinogenesis 16 (1995) 1595–1602.
[6] P. Branch, G. Aquilina, M. Bignami, P. Karran, Defective mismatch binding and a mutator phenotype in cells tolerant to DNA damage, Nature 362 (1993) 652–654.
[7] M. Hidaka, Y. Takagi, T.Y. Takano, M. Sekiguchi, PCNA-MutSalpha-mediated binding of MutLalpha to replicative DNA with mismatched bases to induce apoptosis in human cells, Nucleic Acids Res. 33 (2005) 5703–5712.
[8] A. Kat, W.G. Thilly, W.H. Fang, M.J. Longley, G.M. Li, P. Modrich, An alkylation-tolerant, mutator human cell line is deficient in strand-specific mismatch repair, Proc. Natl. Acad. Sci. U.S.A. 90 (1993) 6424–6428.
[9] B.J. Glassner, G. Weeda, J.M. Allan, J.L. Broekhof, N.H. Carls, I. Donker, B.P. Engelward, R.J. Hampson, R. Hersmus, M.J. Hickman, R.B. Roth, H.B. Warren, M.M. Wu, J.H. Hoeijmakers, L.D. Samson, DNA repair methyltransferase (Mgmt) knockout mice are sensitive to the lethal effects of chemotherapeutic alkylating agents, Mutagenesis 14 (1999) 339–347.
[10] K. Sakumi, A. Shiraishi, S. Shimizu, T. Tsuzuki, T. Ishikawa, M. Sekiguchi, Methylnitrosourea-induced tumorigenesis in MGMT gene knockout mice, Cancer Res. 57 (1997) 2415–2418.
[11] A. Shiraishi, K. Sakumi, M. Sekiguchi, Increased susceptibility to chemotherapeutic alkylating agents of mice deficient in DNA repair methyltransferase, Carcinogenesis 21 (2000) 1879–1883.
[12] T. Tsuzuki, K. Sakumi, A. Shiraishi, H. Kawate, H. Igarashi, T. Iwakuma, Y. Tominaga, S. Zhang, S. Shimizu, T. Ishikawa, et al., Targeted disruption of the DNA repair methyltransferase gene renders mice hypersensitive to alkylating agent, Carcinogenesis 17 (1996) 1215–1220.
[13] H. Kawate, K. Sakumi, T. Tsuzuki, Y. Nakatsuru, T. Ishikawa, S. Takahashi, H. Takano, T. Noda, M. Sekiguchi, Separation of killing and tumorigenic effects of an alkylating agent in mice defective in two of the DNA repair genes, Proc. Natl. Acad. Sci. U.S.A. 95 (1998) 5116–5120.
[14] Y. Takagi, M. Takahashi, M. Sanada, R. Ito, M. Yamaizumi, M. Sekiguchi, Roles of MGMT and MLH1 proteins in alkylation-induced apoptosis and mutagenesis, DNA Repair (Amst.) 2 (2003) 1135–1146.
[15] K. Ochs, B. Kaina, Apoptosis induced by DNA damage O6-methylguanine is Bcl-2 and caspase-9/3 regulated and Fas/Caspase-8 independent, Cancer Res. 60 (2000) 5815–5824.
[16] K. Komori, Y. Takagi, M. Sanada, T.H. Lim, Y. Nakatsu, T. Tsuzuki, M. Sekiguchi, M. Hidaka, A novel protein, MAPO1, that functions in apoptosis triggered by O6-methylguanine mispair in DNA, Oncogene 28 (2009) 1142–1150.
[17] M. Baba, S.B. Hong, N. Sharma, M.B. Warren, M.L. Nickerson, A. Iwamatsu, D. Esposito, W.K. Gillette, R.F. Hopkins 3rd, J.L. Hartley, M. Furihata, S. Oishi, W. Zhen, T.R. Burke, W.M. Linehan Jr., L.S. Schmidt, B. Zbar, Folliculin encoded